NTNU – Trondheim
Norwegian University of
Science and Technology

The Influence of Salts with Different Cation Valency on Oil-in-Water Emulsion Stability
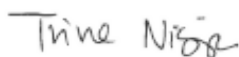
Trine Nisja

Preface

This master thesis concludes my studies at the Department of Chemical Engineering, with specialisation in Colloid and Polymer Chemistry, at the Norwegian University of Science and Technology. The work has been performed at the Ugelstad Laboratory during the spring of 2015.

I would like to thank my co-supervisor Camilla Israelsen Dagsgård for great guidance regarding my work, good discussions, great patience and extraordinary helpful advises on the writing of this thesis. I also want to thank my supervisor, Johan Sjöblom, for highly appreciated guidance throughout the project. Great thanks to May Grete Sætran for her guidance regarding the laboratory set-up and her genuine optimism. In addition, I would like to thank Geir H. Sørland for helping me out with the low-field NMR procedure. Jens Norrmann deserves thanks for good academic discussions regarding my results.

My fellow students and friends deserve great thanks for being awesome – you have made my days! My gratitude also reaches outside the campus of Gløshaugen, and is especially directed towards my beloved parents, Kari and Asbjørn. I am forever grateful for the support, both morally and economically.

I declare that this is an independent work according to the exam regulations of the Norwegian University of Science and Technology (NTNU).

<div align="center">

Trondheim, June 25, 2015

Trine Nisja

Trine Nisja

</div>

ii

Abstract

The effect of different emulsion preparation parameters on the stability of oil-in-water (o/w) emulsions has been studied by varying the preparation parameters and then observing the emulsion visually. Change in the turbidity of an emulsion indicated instability, and the formation of a dense layer on the top of the emulsion suggested that creaming had commenced. The creaming rate was diminishing with increasing mixing frequency, mixing time and oil phase density. The study was limited by foam build-up, as the unwanted foam made it necessary to keep mixing frequency and surfactant amount to a minimum.

The influence of diluted salts of different valencies on the stability of o/w emulsions has been investigated by measuring the zeta potential of emulsions with varying electrolyte concentration and electrolyte cation valency. The destabilising effect of adding divalent Ca^{2+} was stronger than that of Na^+, which was observed by the difference in electrolyte concentration required to reduce the absolute value of zeta potential. This strongly implies that the higher valency of Ca^{2+} more readily contributes to a compression of the electrical double layer than does Na^+. Contrary to expectations, the addition of trivalent Al^{3+} and Fe^{3+} was not observed to affect the stability. It was concluded that this deviation from theory was due to experimental limitations.

A new method for droplet size characterisation and oil profile for w/o emulsions with low-field nuclear magnetic resonance (NMR) has been developed and tested for o/w emulsions in collaboration with the NMR supplier, Antek AS. Implementation of a convection compensating sequence by Antek AS was successful. The new procedure makes it possible to retrieve quantitative data on the droplet size and oil profile of an o/w emulsion over time, which can provide good insight into emulsion stability.

Sammendrag

Effekten ulike parametere for emulsjonspreparering har på olje-i-vann-emulsjoner har blitt studert ved å variere parameterne og deretter observere emulsjonen visuelt. Turbiditetsforandringer i emulsjonen indikerte ustabilitet, og dannelsen av et kompakt lag i toppen av emulsjonen antydet at dråpene har begynt å kreme (omtales heretter som sedimentere). Sedimentasjonshastigheten sank med økende blandingsfrekvens, blandingstid og tettheten til oljefasen. Uønsket skumdannelse begrenset undersøkelsen fordi det ble nødvendig å holde blandingsfrekvensen og mengden emulgator lav for å unngå ytterligere skumdannelse.

Påvirkningsgraden av oppløste salter med ulik kationvalens ble undersøkt ved å måle zetapotensialet til emulsjoner med varierende elektrolyttkonsentrasjon og valens av kationet i elektrolytten. Den destabiliserende effekten av å tilsette divalente kalsiumioner var sterkere enn effekten av å tilsette natriumioner. Dette ble observert ved å se på forskjellen i elektrolyttkonsentrasjon som krevdes for å redusere absoluttverdien til zetapotensialet. Dette impliserer at den høyere valensen til kalsiumioner bidrar sterkere til kompresjon av det elektriske dobbeltlaget enn det de monovalente natriumionene gjør. Tilsetning av trivalente aluminiumioner og jern(III)ioner så ikke ut til å påvirke stabiliteten til emulsjonen ettersom det ikke ble observert noen forandring i zetapotensial. Da dette fraviker fra teorien, ble det konkludert med at avviket skyldes eksperimentelle begrensninger.

En ny metode som kan brukes til bestemmelse av dråpestørrelsesfordeling og oljeprofil til vann-i-olje-emulsjoner ved hjelp av low-field kjernemagnetisk resonans (NMR) har blitt utviklet og testet for olje-i-vann-emulsjoner i samarbeid med leverandøren av NMR-instrumentet, Antek AS. En vellykket implementering av en konveksjonskompenserende sekvens ble utført av Antek AS. Den nye metoden gjør det mulig å hente kvantitative data om dråpestørrelsesfordelingen og oljeprofilen til en emulsjon over tid, noe som kan gi forbedret innsikt i emulsjonsstabilitet.

Contents

1 | Introduction

With a growing world population, energy demand is expected to increase [1]. Oil is a central energy source, and it is becoming more and more important to understand every step of the oil recovery in order to increase the efficiency and ensure maximum recovery from the reservoirs [2]. Both in the reservoir and at different steps of oil recovery and refining processes, emulsions are formed [3], which makes the study of emulsions highly relevant to flow assurance and oil recovery optimisation. The fluid that occurs in an oil reservoir, formation fluids, contains a variety of inorganic compounds, including dissolved salt ions of different valencies [4], which are known to affect the stability of emulsions [5, 6, 7].

In this study, the effect that diluted salts of different cation valency have on the stability of an oil-in-water (o/w) emulsion are investigated by measuring the zeta potential of the emulsion droplets at different concentrations of electrolyte with monovalent or multivalent cations. The addition of salt is expected to destabilise the emulsion due to reduction in electrostatic repulsive forces between the droplets.

In order to perform zeta potential measurements, an o/w emulsion of adequate stability needs to be prepared. To obtain such an emulsion, different parameters of emulsion preparation can be applied, and the effect of varying some of these parameters will be studied by visual observation.

An other way to study the stability of emulsions, is by a low-field NMR method developed by Antek AS in collaboration with NTNU [8]; by modifying the current program for characterising w/o emulsions, it can be applied to o/w emulsions as well.

2 | Theory

2.1 Emulsions

Two immiscible liquids form an emulsion whenever one of the liquids is dispersed into the other liquid as droplets in a continuous medium [9]. The dominating types of emulsions are the ones that contain water as either dispersed or continuous phase [10], and these are referred to as water-in-oil (w/o) and oil-in-water (o/w) emulsions, respectively. In this context, «oil» is any liquid that is immiscible or only slightly soluble in water.

Based on the diameter, d, of the droplets, emulsion systems can be divided into three main groups: Macroemulsions ($d > 1\,\mu m$), miniemulsions ($50\,nm < d < 1\,\mu m$) and microemulsions ($d < 50\,nm$), of which the latter of the three is thermodynamically stable and forms spontaneously due to high entropy contributions [11]. The other two, however, are thermodynamically unstable, and need to overcome an energy barrier in order to break a stable bulk phase into droplets[10].

As the total surface area increases when droplets are formed, so does the total interfacial free energy [10]. Still the dominating part of the energy barrier originates from the increased Laplace pressure that comes with the breaking of large droplets (or bulk phase) into smaller droplets [12]. As soon as the energy supply is cut, the system will go towards a lower energy state by breaking up the emulsion until the two liquids are completely phase separated and only separated by one single interface.

2.1.1 Emulsion preparation

Emulsion preparation, or emulsification, is the breaking up of a bulk phase into small droplets, and this process requires a large supply of energy; the droplets are deformed to such an extent

that it is more energetically favourable to break up into two droplets [12]. The Laplace pressure (see eq. (2.1)), the pressure difference between the concave and convex side of a curved interface, opposes this deformation.

$$\Delta p = P_{\text{inside}} - P_{\text{outside}} = \gamma \left(\frac{1}{R_1} + \frac{1}{R_2} \right) \tag{2.1}$$

Here, P_{inside} and P_{outside} are the pressure inside and outside the droplet, respectively. γ is the interfacial tension, R_1 and R_2 are the radii of curvature. For spherical droplets, (2.1) reduces to:

$$\Delta p = \frac{2\gamma}{R} \tag{2.2}$$

The Laplace pressure must be applied through agitation in order to disrupt a droplet, and this is what requires energy.

Using mechanical stirring for emulsion preparation only results in coarse emulsions [10], so to prepare emulsions with smaller droplets other methods should be used. Alternatives include emulsification by ultrasound[13], homogeniser, and apparatuses equipped with differently shaped dispersing elements that utilises the stator-rotor principle to disperse one phase into the other. Whether the emulsion prepared is a w/o or o/w emulsion depends on many factors, but the main ones are the properties of surfactant(s) used to stabilise the emulsion, and the volume fraction of the phases [10].

2.1.2 Emulsion stability

The droplets in an emulsion will move around due to Brownian motion, and how they interact upon encounter is what determines the emulsion stability. As two droplets are approaching each other, attractive and repulsive forces will start to affect their motion; attractive potential forces, which mainly includes van der Waals forces, trigger aggregation, whereas repulsive forces (electrostatic or steric forces) enforce the stability of an emulsion. The opposing forces generate attractive and repulsive potential energy, V_A and V_R respectively, which add up to the total potential energy of the system(V_T). The magnitude of the potential energy change with respect to the distance between the droplets is shown in Fig. 2.1.

The plot shows two minima and one maximum (V_{max}), where $V_A > V_R$ at both the minima and $V_R > V_A$ at the energy maximum [14]. The minimum at large interparticle distances, the secondary minimum, is considered to represent reversible flocculation; at this point, the attractive
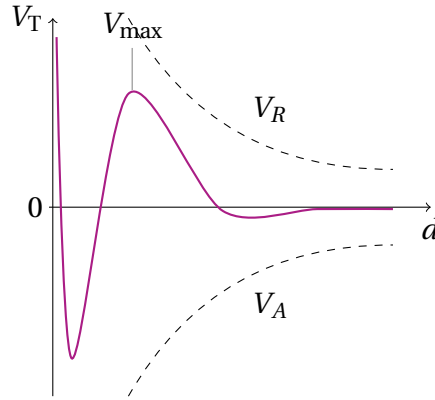
Figure 2.1: Potential energy curve for two approaching particles. Total interaction energy , V_T, of the system as a function of distance of separation, d. The attractive (V_A) and repulsive (V_R) potential energies are also shown separately.

forces are slightly dominating, and consequently, loose, reversible aggregates may be formed. This, however, is only applicable for relatively large droplets. As the droplets approach each other further, their electrical double layers (see Section 2.1.3) start to overlap. This is when the repulsive forces start to prevail, causing the total interactin energy to rise towards a maximum. The magnitude of V_{max} is equivalent to the energy barrier of coagulation and depends on the range of the repulsive forces as well as the zeta potential of the droplets [15]. Whenever two approaching droplets move close enough for the attractive van der Waal forces to predominate the repulsive forces, and thus overcome V_{max}, they will reach the deep, primary minimum resulting in irreversible aggregation and loss of kinetic identity [10].

The time a system requires to break an emulsion is, in difference from the thermodynamics, possible to alter. This makes it possible to make emulsions that are kinetically stable for relatively long time spans (up to decades) as they exist in a metastable state where the energy barrier to aggregation is high enough to resist the emulsion breaking process [11].

Kinetic stability can be affected in several ways, the key is to look into the emulsion breaking mechanisms:

- Lower the interfacial tension, which lowers the energy gained from coalescence.

- Increase the elasticity of the interfacial film (Gibbs-Marangoni effect)[12].

- Increase the mechanical strength of the interfacial film through strong intermolecular forces in condensed monolayer[10].

- Increased viscosity of the continuous phase, which reduces the mobility of the droplets.

- Lower volume fraction of the dispersed phase, reduces the frequency of droplet collision.

- Narrow droplet size distribution, increases the resistance against molecular diffusion (Ostwald ripening).
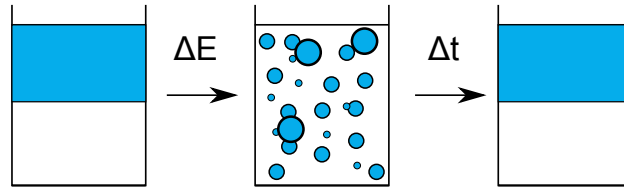

Figure 2.2: Illustration of emulsion stability. Energy is supplied to break one phase (dispersed phase) into droplets. Over time, the thermodynamic instability of the emulsion will cause phase separation.

One of the ways to reduce the interfacial tension is to add a surface-active agent (surfactant) that has a strong tendency to adsorb on the interface due to its amphiphilic properties. A surfactant molecule will orient its hydrophilic part into the water phase and hydrophobic part into the oil phase, which reduces the interfacial tension and increases the kinetic stability of an emulsion. The surfactant may be nonioinic, anionic, cationic or zwitterionic, where the latter has both a cationic and anionic part of the hydrophilic head. In addition to reducing the interfacial tension, ionic surfactants contribute to an electrostatic stabilisation of the droplets [10].

As a rule of thumb, the phase that the surfactant has the greatest affinity towards, becomes the continuous phase [16]. Other additives that may affect the stability of an emulsion are polymers and non-soluble particles, both of which adsorb to the interface. Polymers mainly contribute to steric stabilisation, whereas solid particles accumulate in the interfacial film due to their wetting properties. The adsorbed particles increase the mechanical strength of the interfacial film [17]. Crude oil emulsions are naturally stabilised by different indigenous compounds. These compounds include asphaltenes, resins, organic acids (e.g. naphtenic acids) and bases [9], as well as stabilising particles [17].

2.1.3   The electrical double layer

In emulsions, surface charge arises in the surface of a droplet that originates from surfactants residing in the interface. Such a charged colloidal particle immersed in polar medium will attract ions of opposite charge (counter-ions), and as a result the concentration of counter-ions is higher near the surface of the particle than the corresponding concentration in the bulk phase. Due to thermal motion, the counter-ions will not accumulate at the surface, but instead form

an ionic cloud surrounding the particle, often referred to as the diffuse double layer [14, 18] or electrical double layer [3].
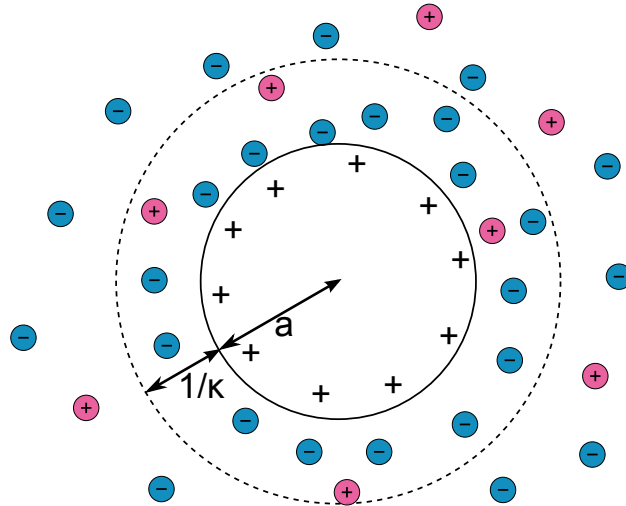
Figure 2.3: Illustration of Gouy-Chapman's model of the electrical double layer surrounding a charged particle.

The concentration gradient of counter ions near the surface of a droplet leads to electrical potential ψ. The potential decreases with increasing distance from the surface until, at a finite distance, the constant bulk concentration is reached [14]. At this point, the charges are in equilibrium and $\psi = 0$. Poisson's equation [10] describes this variation in electrical potential as a function of the net volumetric charge density (ρ) and the permittivity of the medium (ϵ).

$$\nabla^2 \psi = -\frac{\rho}{\epsilon} \tag{2.3}$$

For low surface potentials, the Debye-Hückel approximation can be applied [10]:

$$\left| \frac{ze\psi_0}{2k_B T} \right| << 1 \tag{2.4}$$

where z is the valency of the counter-ion, e is the electron charge, ψ_0 is the surface potential, k_B is the Boltzmann constant and T is the temperature. Combining Poission's equation with Boltzmann's law in the Debye-Hückel approximation results in an equation for the potential distribution around a spherical surface [10]:

$$\psi = \psi_0 \left(\frac{a}{r} \right) \exp\left[-\kappa(r - a) \right] \tag{2.5}$$

where a is the particle radius, r is the distance at any point from the center of the particle and κ is the Debye-Hückel parameter.

κ is one of the most important quantities from this derivation, as it is used to describe the electrical double layer [19]. The inverse of κ is often referred to as the double layer thickness [10, 20] due to its units of reciprocal length, even though the potential gradient actually extends to a distance of about $3/\kappa$ before it has reached 2 % of the surface potential. κ can still be used to compare the relative magnitude of double layers in different systems, and can in this sense be used as a quantitative characterisation parameter of the electrical double layer.

Gouy proposed a simple model for calculations on the diffuse part of the electrical double layer that was further developed by Chapman. Their model is built on the assumptions that the layer could be considered flat, with uniformly distributed surface charge, and it can be compared to a capacitor. One of the limitations of the Gouy-Chapman model, is the assumption that the ions in the diffuse layer is considered as point charges of zero spatial extent. This is not feasible with reality when the surface potential is high, so a new model was developed by O. Stern as illustrated in Fig. 2.4. The Stern model accounts for the fact that the ions take up a certain volume in space. The diffuse part of Stern's electrical double layer model is divided into two parts: The Stern layer ($h < \delta$) and the Gouy Chapman layer ($h > \delta$). In the Stern layer, the ions are adsorbed to the droplet surface and move along with the droplet. The adsorbed counter-ions neutralise some of the surface potential, so the potential declines rapidly between ψ_0 and ψ_δ. At distances higher than δ, the diffuse layer behaves as originally described by Gouy-Chapman when ψ_0 is replaced by ψ_δ [10].
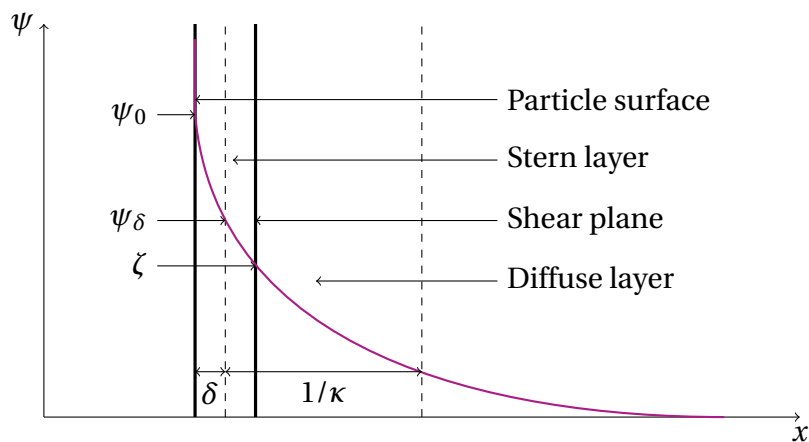

Figure 2.4: Schematic illustration of Stern's electrical double layer model with potential, ψ, as a function of distance from the particle surface, x. ψ_0 is surface potential, ψ_δ is Stern potential, ζ is the zeta potential, δ represents the radius of an adsorbed ion and κ is the Debye-Hückel parameter.
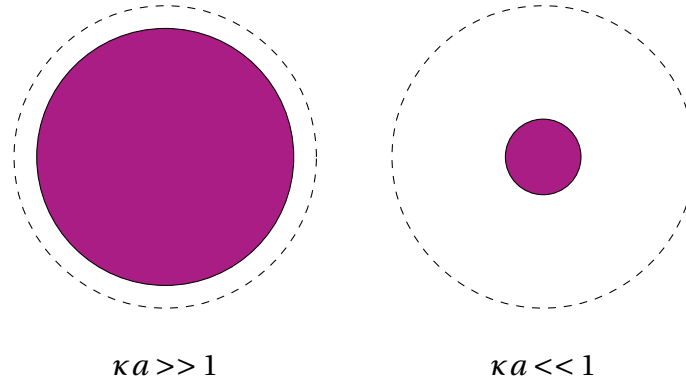
$\kappa a \gg 1$ $\kappa a \ll 1$

Figure 2.5: Illustration of a charged particle with a thin double layer ($\kappa a \gg 1$) and one with a thick double layer $\kappa a \ll 1$

The magnitude of surface potential can not be measured directly, but measuring electrokinetic effects can give an indication of ψ_0 through the zeta potential, which is assumed to be approximately equal to the Stern potential [10]. Within the electrical double layer, the zeta potential (ζ) is the potential at the plane of shear (see Fig. 2.4), an imaginary surface laying close to the particle surface. The fluid between the plane of shear and the particle surface is considered to be stationary[18], and will accordingly move along with the particle as they together form a kinetic unit. This is why measurements of the electrophoretic mobility of such a particle does not give a measure of the actual surface charge of the particle, but rather the net charge of the particle, corresponding to the charge at the shear plane.

ζ is related to electrophoretic mobility (μ) by Smoluchowski's equation (Eq. (2.6)) or Hückel's equation (2.7), depending on the relative thickness of the double layer; if the charged particle has a thin double layer ($\kappa a \gg 1$), Smulochowski's equation is applied, and Hückel's equation is applied when the double layer is thick ($\kappa a \ll 1$) [14].

$$\mu = \frac{\epsilon_r \epsilon_0}{\eta} \zeta \tag{2.6}$$

$$\mu = \frac{2\epsilon_r \epsilon_0}{3\eta} \zeta \tag{2.7}$$

Here, μ is the electrophoretic mobility, ϵ_0 is the permittivity of free space, ϵ_r is the dielectric constant of the dispersion media, η is the dynamic viscosity of the dispersion medium.

2.1.4   Electrokinetic effects

Whenever they are exposed to an electrical field, particles that have electrically charged surfaces will exhibit certain effects named electrokinetic effects:

- Electrophoresis: An applied electrical field causes the movement of a charged particle relative to the liquid in which it is suspended.

- Electroosmosis: An applied electrical field causes the movement of a liquid relative to a stationary charged surface.

- Streaming potential: An electrical field is generated from forcing a liquid to flow along a charged surface.

- Sedimentation potential: An electrical field is generated from the movement of charged particles relative to a stationary liquid.

When a charged particle surrounded by an electric double layer is exposed to an electric field, the double layer is distorted and as a consequence creates its own electric field [21]. This electric field opposes the electrophoretic motion of the particle to a magnitude related to the thickness of the electrical double layer. The opposing field thus slows down the particle motion through the liquid, and the phenomenon is accordingly named the electrophoretic relaxation effect[21].

2.1.5   Ionic strength

The zeta potential of an emulsion depends on the amount and valency of any ions present, and an important characteristic of a salt solution (electrolyte) is its ionic strength. The ionic strength of an electrolyte can be calculated using the following equation [22, 23]:

$$I = \frac{1}{2} \sum_{i=1}^{n} C_i z_i^2 \tag{2.8}$$

where I is the ionic strength, C_i is the molar concentration of ion i and z_i is the charge number of ion i. From Gouy-Chapman theory, a correlation between ionic strength and the Debye length (κ^{-1}) can be derived:

$$\kappa = \left(\frac{2000F^2}{\epsilon_0 \epsilon_R RT} \right)^{\frac{1}{2}} \sqrt{I} \tag{2.9}$$

Here F is the faraday of charge (the magnitude of the charge on a mole of electrons), R is the gas constant per mole and T is the temperature of the system. From (2.9), it can be seen that the Debye length is inversely proportional to the square root of the ionic strength. This means that the double layer will be compressed by increasing the concentration or valency of counter-ions in the system [10]. The critical coagulation concentration (CCC) is the concentration of a given salt that is required to make a dispersed system coagulate due to loss in electrostatic stability[3]. According to the Schultze-Hardy rule, the concentration and valency of the counter-ion (relative to the droplet surface charge) in an electrolyte has the greatest effect on reducing the absolute value of the relative surface charge [10]. Quantitatively, it states that the CCC varies inversely with the sixth power of the counter-ion charge number, z [3].

2.1.6   Breaking of emulsions

As emulsions in the colloidal size range are thermodynamically unstable, they will eventually be subject to phase separation. The process of demulsification can be divided into two main steps: The first step is a change in position of the droplets without affecting the size or number of droplets in the emulsion. In the second step, the average droplet size increases due to either Ostwald ripening or coalescence. An overview of the mechanisms is given in Fig. 2.6.

The first step consists of two mechanisms that are based on gravitational force, creaming (Fig. 2.6b) and sedimentation (Fig. 2.6d), which depends on the density of the dispersed phase and continuous phase. When the particles are very small, which often is the case in colloidal systems, the gravitational force on each particle is negligible due to the stronger effect of entropy; high entropy is thermodynamically favourable, so the spreading of particles through diffusion becomes the dominating mean of particle motion [19]. If the attractive forces are strong enough, flocculation (Fig. 2.6c) can occur upon particle encounter. Neither of these mechanisms directly affect the size of the particles in the system, however, they promote coalescence by increasing the droplet crowding and thus the probability of droplet-droplet collision[10].

In the second step, the emulsions are broken down into larger droplets and, eventually, separated into two phases. Ostwald ripening (Fig. 2.6e), or molecular diffusion, is a process in which the high Laplace pressure difference in small droplets forces molecules to diffuse out of the smaller droplets through the continuous phase and into larger droplets with lower Laplace pressure. This process is highly dependent on the viscosity of the continuous phase, as molecular mobility decreases with increasing viscosity. How strong the repulsive forces between the molecules in the dispersed phase are towards the molecules in the continuous phase is another factor that
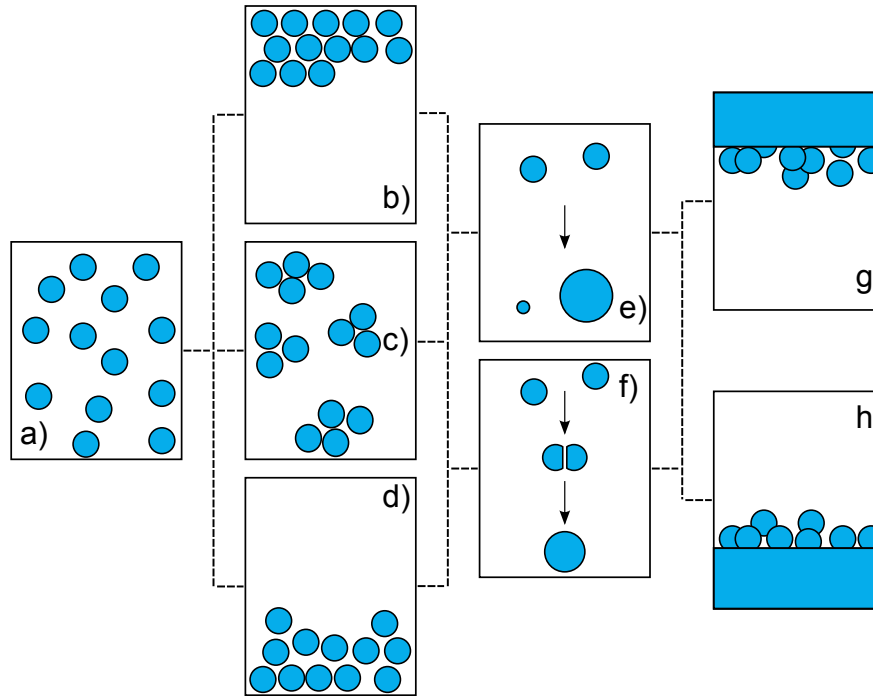
Figure 2.6: Mechanism of emulsion breaking. a) uniform emulsion; b) creaming; c) aggregation; d) sedimentation; e) Ostwald ripening; f) coalescence; g) and h) phase separation.

affects the diffusivity. Lastly, coalescence (Fig. 2.6f)is the merging of two or more droplets into one larger droplet. This requires the droplets to approach each other, leading to a deformation of the droplets that, if the energy is strong enough, causes fluctuation in the liquid film between the droplets. The droplets rupture as the film collapses due to the film reaching a critical thickness [14].

Emulsion formation can cause problems in the oil industry partly due to the salt content of produced water, which is corrosive, as well as difficulties with purifying the oil before refining. To solve these issues, methods that break up emulsions have been developed, all depending on what stabilises the emulsion. These methods can be divided into three groups: Mechanical, chemical and electrical destabilisation. Mechanical destabilisation includes simple sedimentation, centrifuge, membrane and other ways of applying shear force to break the emulsion. Addition of chemicals that reduce the stability by rupturing the protective film, stabilise the opposite kind of emulsion or compress the electrical double layer and thus reduce the repulsive forces between the droplets can also be done. Lastly, by applying an electrical field, droplets with polar or induced polar properties can be deformed and collapse due to the corresponding increase in surface area [24].

2.2 Foams

A sudden large increase of the contact area between gas and liquid can be the origin of foam production[25]. Foams are dispersions of gas in a solid or liquid continuous phase, and they are confusingly similar in behaviour to highly concentrated emulsions [10]. Consequently, surfactants that are good emulsifying agents usually are good foaming agents as well [15], which can be a challenge in systems where one of the two is undesired. To prevent foaming, foam inhibitors or antifoams may be added to the system, both of which prevent foaming agents from stabilising the foam[19].

2.3   Emulsion characterisation

2.3.1   Optical microscope

Optical microscope imaging is used for direct observation of a sample, and can be used to measure particles in the colloidal size range. The details of an object is dissolved by a collection of lenses in the microscope which transfers a magnified image to the observer [26]. Optical microscopy can observe objects down to nano scale, the lower limit depending on the optical contrast between the particles and the environment [10], light source or use of fluorescence [27]. Limitations of optical microscope imaging include the need of a sample to be transparent. Further, the sample must be spread out on a plate and possibly be diluted, which may disrupt the emulsion. Lastly, only small parts of a sample are measured, which may not be representative for a non-uniform emulsion.

2.3.2   Low-field nuclear magnetic resonance

A method using low-field nuclear magnetic resonance (NMR) to determine quantities like droplet size distribution (DSD) and water profile in an emulsion has been developed at NTNU [8, 28]. Advantages with this method include that it measures the entire emulsion sample, and that the light absorption of the sample is not relevant, in difference from optical microscopy. Moreover, since the sample is observed in a relatively large (diameter = 15 mm) glass tube, the possibly disrupting preparation methods that are necessary for characterisation in microscope are avoided.

The difference in viscosity between the two phases in an emulsion are what is utilised by the NMR program, as it yields a difference in longitudinal (T_1) and/or transverse (T_2) relaxation times when the emulsion is subjected to NMR [29]. By suppressing the oil signal, relaxation time distributions of water alone is obtained, as illustrated in Fig. 2.7, where T_2 distribution with and without suppression of the oil signal is demonstrated. The T_1 and T_2 distributions can, together with the diffusion coefficient obtained from the difference in molecular mobility of the phases, be used to calculate the DSD in absolute length units [8] as well as water profile of an w/o emulsion [28].
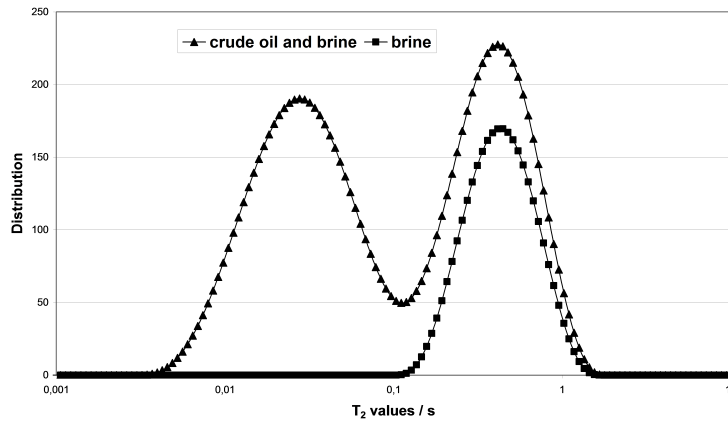
Figure 2.7: T_2 distributions of a water in crude oil emulsion system with (1 peak) and without (2 peaks) suppression of the oil signal.

Sample convection

Particles that are dispersed in a continuous media will, to a certain degree, be subject to random movement called Brownian motion due to the particle colliding with the small liquid molecules that build up the continuous media [30]. The liquid molecules move spontaneously due to thermal motion. The distance travelled by random Brownian motion of the molecules is measured over the observation time, D5, to determine the self-diffusion coefficient, which is used to calculate the droplet size distribution. A challenge with diffusion measurements using low-field NMR is that they are easily disrupted by non-Brownian motion, such as Rayleigh-Bénard convection that arises from temperature gradients in the sample [29]. Rayleigh-Bénard convection is fluid motion that occurs in a plane horizontal layer of fluid that is heated from below. As Fig. 2.8 demonstrates, the temperature gradient originating from the heating causes the fluid to form Bénard convection cells [30]. The effect of convection is particularly relevant to diffusion experiments in low-viscosity experiments, such as oil-in-water emulsions, where the molecules are more free to move than in higher viscosity systems.

One solution that can be applied to make up for sample convection is to raise the critical Rayleigh number, Ra_c, by implementing smaller sample dimensions [29], since fluid motion due to thermal convection only occurs for $Ra > Ra_c$. Another solution is to introduce so-called convection compensating pulsed field gradient NMR sequences. Such sequences deal with the disruptions by suppressing the effects caused by convection.
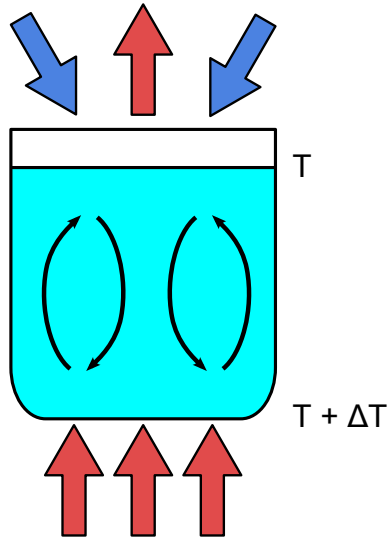
Figure 2.8: Illustration of Rayleigh-Bénard convection.

2.3.3 Zetasizer

The zeta potential of the emulsion droplets can be measured using an electrophoresis system as shown in Fig. 2.9 combined with laser doppler velocimetry. An electrical potential is applied to the electrodes, making charged particles move towards the electrode of opposite charge. When a laser beam is directed on the sample, the particles scatter the light from the beam and the scatter is measured by a detector. The scattered light produces a fluctuating intensity signal that has a rate of fluctuation proportional to the speed of the particles. The speed corresponds to the electrophoretic mobility of the suspended particles[20].
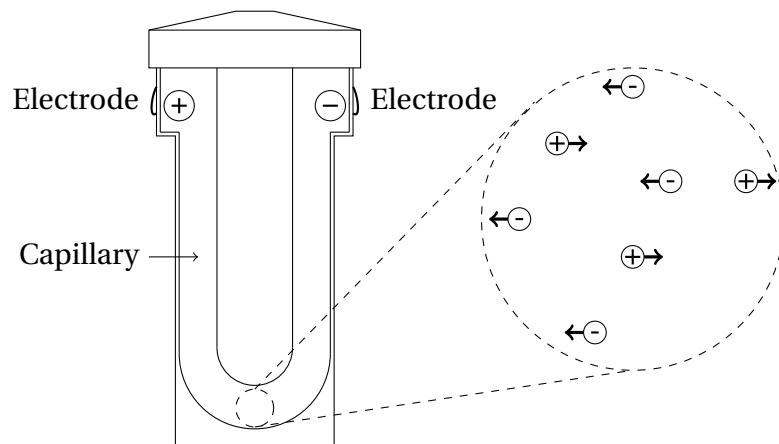
Figure 2.9: Electrophoresis cell with electrodes. Charged particles are diffusing towards the electrode of opposite charge.

2.3.4   Visual observation of emulsions

The size and distribution of particles affects the appearance of emulsions and other colloidal dispersions due to light scattering of the dispersed particles, a phenomenon called the Tyndall effect. The turbidity of an emulsion reflects the droplet size; large droplets scatter results in a milky-white-opaque appearance, and as the droplet size decreases, the emulsion changes to blue-white, grey-translucent, and finally, transparent (micro emulsion droplets). This phenomenon makes it possible to study an emulsion qualitatively by visual observation.

3 | Experimental

The experimental procedures that were used in this project are described in this chapter. The first part of the project was to test the influence of different parameters on the preparation of stable oil-in-water (o/w) emulsions. An o/w emulsion that seemed to be satisfyingly stable was further used for zeta potential analysis to determine the effect of different electrolytes on emulsion stability. To quantify emulsion stability, a method for water-in-oil (w/o) emulsion characterisation using low-field NMR was customised and tested for o/w emulsions. All of the experiments were conducted at room temperature (25 °C).

3.1 Preparation of oil-in-water emulsion

3.1.1 Choice of components

Simple alkanes of high purity were chosen as the dispersed oil phase for the emulsions and Milli-Q water (18.2 MΩ cm at 25 °C) was used for the continuous phase. Properties of the emulsion components are given in Table 3.1.

Table 3.1: Density, viscosity and solubility in water of the emulsion components at 25 °C. The viscosity data and solubility data are obtained from the safety data sheet of the respective component. Solubility is reported as mass component soluble per volume water at 20 °C, i = practically insoluble.

Component	Density [31] $[\mathrm{g\,cm^{-3}}]$	Viscosity $[\mathrm{mPa\,s}]$	Solubility $[\mathrm{g\,l^{-1}}]$
Heptane	0.680	0.39	0.05
Decane	0.726	0.92	i
Hexadecane	0.851	3.04	i
Water	1.000	0.89	

Sodium dodecyl sulfate (SDS) was chosen as emulsifying agent because of its electrostatic stabilising properties and anionic nature. Its affinity towards water makes SDS suitable for stabilising o/w emulsions, and SDS has been reported to greatly reduce the surface tension of hydrocarbon-water interfaces [32]. This was especially applicable to SDS concentrations below the critical micelle concentration (CMC) of 8.1×10^{-3} moll^{-1} [32]. In some of the emulsions, decanol was used as a co-surfactant (foam inhibitor) to reduce the amount of foam.

3.1.2   Mixing

The emulsions were prepared using an Ultra-Turrax disperser (IKA, T18, 10 mm head), an electronic overhead stirrer (IKA, 4-bladed propeller) or a horizontal mechanical shaker, depending on the desired mixing frequency. The mechanical shaker was used for mixing frequencies lower than 500 revolutions per minute (rpm), the propeller for 500 to 2000 rpm and the Ultra-Turrax for frequencies higher than 3000 rpm.

Each emulsion was prepared in a glass vial, with a total liquid volume of 30 ml. The experimental set-up is shown in Figure 3.1.
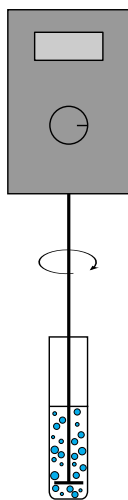

Figure 3.1: Set-up for mixing.

3.1.3   Emulsion stability

After preparation, the emulsions were observed over time in the glass vials they were prepared in, and any change in the turbidity of an emulsion was recorded. Some of the emulsions were

also studied in an optical light microscope to confirm that an emulsion had been created.

3.2 Zeta potential measurements

The electrophoretic mobility of the oil droplets in an emulsion was measured using a Malvern Zetasizer Nano ZS [20], referred to as Zetasizer. The Zetasizer software provided by Malvern UK was used to monitor the experiment, and Smoluchowski's model was used by the software to calculate the zeta potential, ζ, from the measured electrophoretic mobility. The temperature for the measurements was set to 25 °C and the refractive indexes used in the model was 1.434 and 1.330 for hexadecane and water, respectively.

The zeta potential at different pH values was measured, and subsequently, the pH was kept constant as salt solutions with cations of different valency was added to the emulsion.

3.2.1 General procedure

A stock emulsion was prepared with a hexadecane volume fraction of 10 % and an SDS mass of 0.5 g per 100 g hexadecane. The emulsions were mixed using an Ultra-Turrax disperser; the oil was added to the water phase while mixing at a frequency of 3000 rpm, and then the two phases were mixed for 1 minute at 8000 rpm. A portion of the stock emulsion was used to make a diluted emulsion with an oil fraction of 0.05 % and an SDS concentration of $6.7\,\mu\mathrm{mol\,l^{-1}}$.

Following on, the pH of the diluted emulsion was measured by a pH-meter and adjusted by the addition of dilute acid (HCl) and base (NaOH). A 3 ml syringe was used to fill a clear, disposable zeta cell cuvette with the diluted emulsion, and the cuvette was put into place in the Zetasizer. The cuvette was cleaned with ethanol and Milli-Q water between each parallel.

3.2.2 Zeta potential measurements with varying pH

The first zeta potential measurements were conducted with pH as the variable. The emulsions were prepared and then diluted with Milli-Q water to an oil volume fraction of 0.05 %. Two different procedures were tested for the next step of the experiment:

1. A portion of the diluted emulsion was transferred to a glass vial, and the pH for this sample was adjusted to pH = 2. Next, the emulsion was analysed by the Zetasizer. When the mea-

surement for that sample was finished, a new portion was taken from the diluted emulsion to prepare the next sample. This was repeated for pH = 2, 4, 6, 8 and 10.

2. The diluted emulsion was distributed into five small glass vials, one for each pH value, immediately after the diluted emulsion was prepared. The pH was then adjusted for one of the samples, and the sample was shaken before it was analysed by the Zetasizer. This was repeated for pH = 2, 4, 6, 8 and 10.

The main difference between the two procedures is that in the first procedure, each sample was taken from the diluted emulsion with half-an-hour intervals due to the time consuming adjustment of the pH. In the second procedure, the diluted emulsion was distributed into the samples at the same time.

3.2.3   Zeta potential measurements with varying electrolyte concentration

The salt concentration was varied by diluting the stock emulsion with electrolyte of the desired concentration instead of using Milli-Q water. The pH was measured and adjusted to pH = $8.0 \pm$ 0.2 before the sample was analysed in the Zetasizer.

Table 3.2 shows the solubility data of the salts in water.

Table 3.2: Solubility data for the added salts and their corresponding hydroxides at 25 °C[31], i = practically insoluble.

Component	Solubility $\left[g/100\,g \right]$	Hydroxide solubility $\left[g/100\,g \right]$
NaCl	36	114
$CaCl_2$	83	0.12
$AlCl_3 \cdot 6\,H_2O$	45	i
$FeCl_3 \cdot 6\,H_2O$	50	i

3.3   Low-field NMR

3.3.1   NMR convection elimination

The low-field NMR instrument has previously only been used for analysis of w/o emulsions. In order to create an NMR program for o/w emulsions, several tests were necessary so to elimi-

nate the NMR signal originating from convection. Throughout the tests, the NMR sequence was modified by the supplier, Antek AS, by adding a signal sequence that compensated for the sample convection. To test if the diameter of the NMR tube was of significance to the sample convection effect (see Section 2.3.2), a narrower NMR tube (0.8 mm diameter) and a custom designed teflon quadruple sample divider added to a standard NMR tube was each tested at different observation times (D5 values), as potential substitutes for the standard NMR tube (15 mm diameter). To test the effect of the modifications, water samples were measured for different D5 values, and different number of scans.

3.3.2 Emulsion characterisation

A similar hexadecane-in-water emulsion as used as stock emulsion for zeta potential analysis was characterised by using the modified low-field NMR program. After preparation, 3.65 ml of the stock emulsion was transferred to a 1.5 mm NMR tube, which was inserted into the NMR instrument to determine SDS and water profile.

4 | Results

The experimental results have been divided into three sections: Firstly, one that describes the stability of oil-in-water (o/w) emulsions prepared with different oil phase components and preparation parameters; secondly, one that presents the oil droplet zeta potentials that resulted from adjusting pH and electrolyte concentration of an emulsion; and finally, a section where the process of convection elimination of a low-field NMR procedure to customise it for o/w emulsions is presented.

4.1 Emulsion preparation

In order to produce an emulsion that was suitable for stability analysis, preparation parameters such as mixing frequency, mixing time and oil content have been varied. Most of the emulsions showed a similar trend; the emulsion was uniformly milky-white immediately after preparation and separated into a milky-white top layer, a grey-translucent middle layer and a transparent bottom layer as depicted in Fig. 4.1. The layers in some of the emulsions were visually observed to stay unchanged for more than 24 hours.

An emulsion similar to those used for zeta potential analysis was characterised by low-field NMR to get a better impression of the stability.

Emulsions were prepared with heptane as the oil phase, but the first samples prepared were stopped during preparation and discarded due to excessive foaming during the mixing, so therefore the amount of sodium dodecyl sulfate (SDS) was reduced from 30 % of the oil mass (1 % of the total emulsion mass) to 1 % of the oil mass. Most of the heptane emulsions (see Table 4.1) showed visible creaming in less than 5 min, by forming the layers described in Fig. 4.1. Some of the emulsions prepared at high mixing velocities, sample 7 and 9, were stable. On the other hand, those samples also produced the greatest amount of foam.

Figure 4.1: Oil-in-water emulsions immediately after preparation (left) and after layers have formed (middle). Illustration of the formation of emulsion layers (right).

Decane was introduced to replace heptane as the oil phase, due to its higher density, which was expected to reduce the creaming rate. The overall result was better stability, but also higher amount of foam. Data is shown in Table 4.2

A further increase in oil phase density was introduced by using hexadecane as oil phase. The preparation properties and results are shown in Table 4.3. Most of the emulsions looked homogeneous directly after preparation, however creaming was visually observed in less than 5 min in several of the samples. The amount of foam increased with increasing mixing frequency.

Table 4.1: Mixing frequency, mixing time, foam amount produced and stability of heptane-in-water emulsions. Heptane volume fraction was 5 %. The stability is classified as I (visible creaming immediately after preparation), U (visible creaming in less than 5 min) or S (no visible creaming for at least 10 min).

#	Mixing freq. [rpm]	Mixing time [min]	Foam [cm]	Stability
1	300	30.0	1	I
2	3000	1.5	0	I
3	3000	15.0	0	I
4	6000	1.5	0	I
5	6000	5.0	1	I
6	7000	5.0	1	I
7	8000	5.0	2	S
8	8000	5.0	1	I
9	24000	1.5	3	S

Table 4.2: Mixing frequency, mixing time, foam amount produced and stability of decane-in-water emulsions. Decanol as cosurfactant (content 1:1 with SDS). The stability is classified as I (visible creaming immediately after preparation), U (visible creaming in less than 5 min) or S (no visible creaming for at least 10 min).

#	Oil content [wt%]	Mixing freq. [rpm]	Mixing time [min]	Foam [cm]	Stability
1	30	4000	5	2	I
2	30	6000	5	2	S
3	30	6000	5	2	S
4	20	6000	5	-	U
5	20	8000	5	2	S

Table 4.3: Preparation parameters and stability results for hexadecane-in-water emulsions. Some emulsions also contained decanol as cosurfactant (1:1 with SDS amount). Hexadecane volume fraction was 30 %. The stability is classified as I (visible creaming immediately after preparation), U (visible creaming in less than 5 min) or S (no visible creaming for at least 10 min).

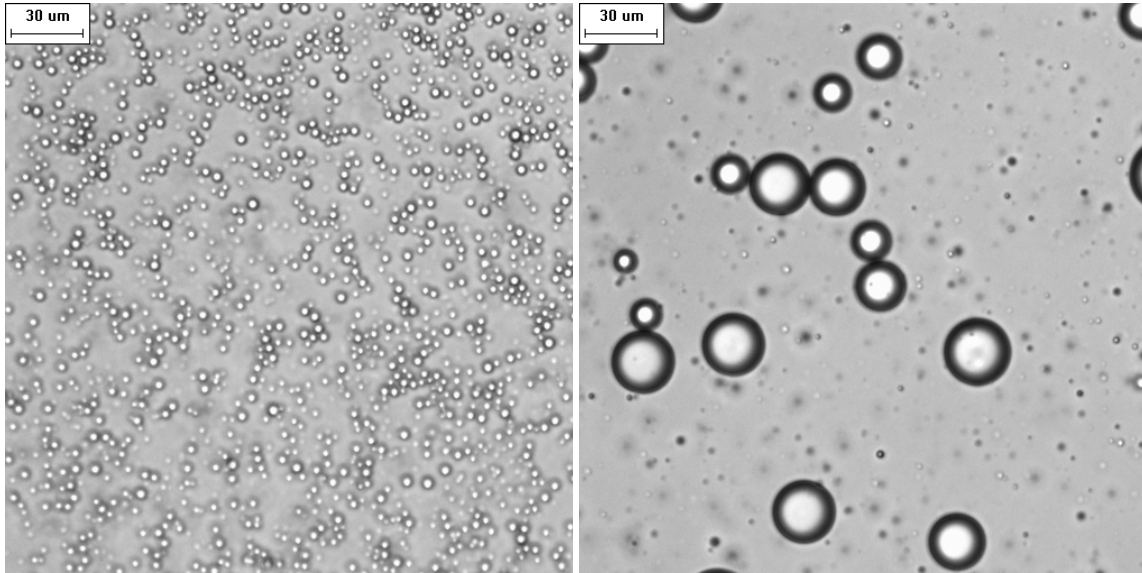| #	Cosurfactant	Mixing freq. [rpm]	Mixing time [min]	Foam [cm]	Stability
1	no	300	30	1	I
2	no	500	27	0	I
3	yes	1500	30	1	I
4	yes	1500	15	1	I
5	yes	1500	10	1	I
6	yes	1500	5	1	I
7	no	2000	5	2	I
8	no	4000	15	2	U
9	yes	4000	5	2	U
10	no	6000	10	2	U
11	no	6000	5	2	U
12	yes	6000	5	1	S
13	no	8000	1	2	S

Figure 4.2: Microscopic images of stock emulsion 1 h after preparation. The left image is of the middle layer and the right image is of the middle layer after turning the emulsion. The emulsion was prepared at 8000 rpm for 1 min with a hexadecane volume fraction of 10 %, and 5 mg SDS per gram hexadecane. The size tag is 30 μm.

The emulsion chosen for the zeta potential analysis was 10 % hexadecane-in-water with 5 mg SDS per gram hexadecane. It appeared to be sufficiently stable from visual observation and had an acceptable amount of foam. Fig. 4.2 shows microscope pictures of the middle layer of the emulsion one hour after preparation. Most of the droplets in the middle layer were in the diameter range of 1 μm to 3 μm. When the sample had been turned a couple of times to mix the layers, larger droplets with diameter of 50 μm were observed in the microscope. The droplet size distribution shown in Fig. 4.3b confirms the presence of these and even larger droplets in the emulsion. Fig. 4.3a shows the oil profile measured using low-field NMR, and the emulsion appeared to have an oil content of up to 60 % in the top of the sample immediately after preparation, and a decreasing oil content in the bottom of the sample.
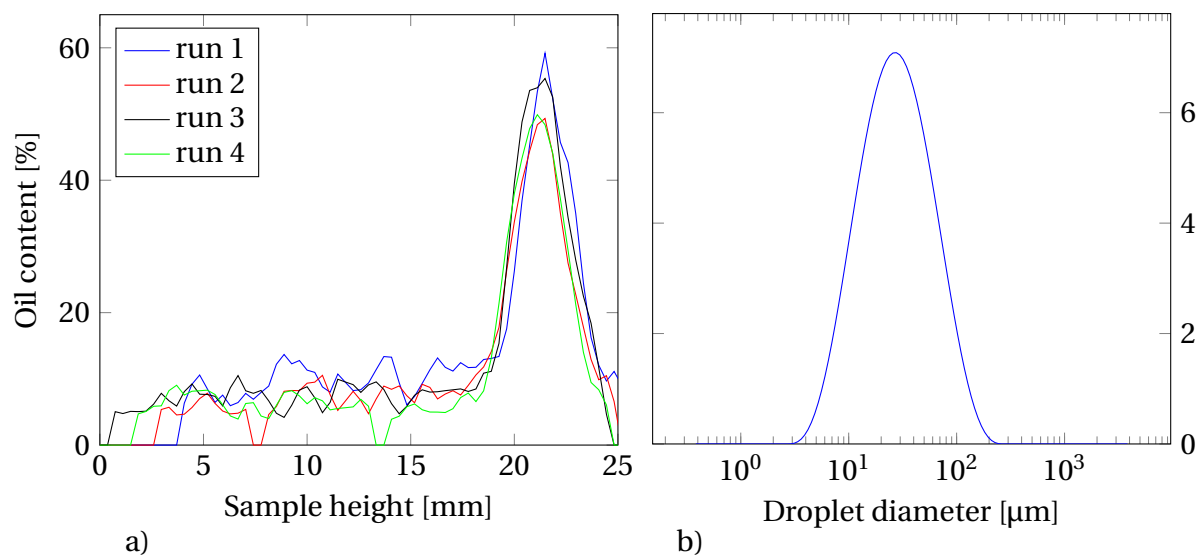
Figure 4.3: a) Oil profile and b) droplet size distribution of hexadecane-in-water emulsion with hexadecane volume fraction of 10 % and SDS as surfactant. Measurements by low-field NMR.

4.2 Zeta potential

The zeta potential of the droplets in an emulsion gives an indication of the electrostatic stability of the emulsion. In the first part of this section, the pH was varied to get an overview of the zeta potential dependency on pH. Further on, the zeta potential was measured while varying the concentration of monovalent, divalent and trivalent chloride salts, respectively. The latter was to study how strongly the degree of valency affected the zeta potential.

Data tables to compliment the results in this section are included in Appendix A.

4.2.1 Zeta potential as a function of pH

The zeta potential of an emulsion prepared as described in Section 3.2.1 was measured while changing the pH value. The first step was to develop a repeatable procedure for manually changing the pH and measuring the zeta potential for each pH, and two procedures (see Section 3.2.2) were tested. The zeta potential measurements from the first procedure, where the portions for dilution were taken from the stock emulsion subsequently, are shown as a function of pH in Fig. 4.4a.
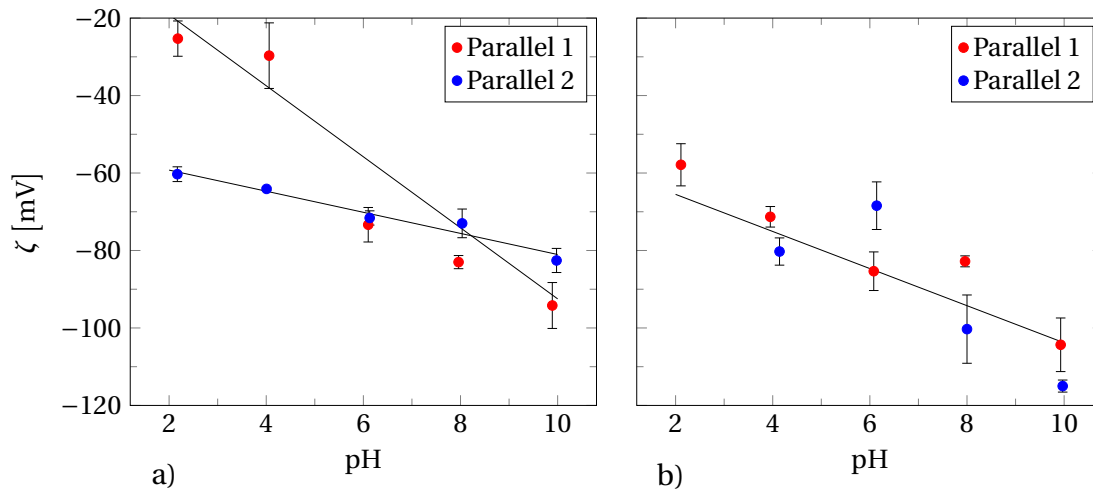

Figure 4.4: Zeta potential (ζ) as a function of pH value. a) First procedure. b) Second procedure

The trend of the two parallels for this procedure were quite diverse, still both showed an increase in the absolute value of the zeta potential, $|\zeta|$, with increasing pH. Linear regression of the two parallels in the first procedure resulted in Eqs. (4.1) and (4.2).

$$\zeta = -9.17\text{pH} - 0.79 \tag{4.1}$$

$$\zeta = -2.72\text{pH} - 53.80 \tag{4.2}$$

The second procedure, where the stock emulsion was distributed for all the dilutions simultane-
ously immediately after preparation, was tested as an alternative to the first procedure, and the
resulting ζ is shown as a function of pH in 4.4b. Linear regression was carried out for the average
of the two parallels, since the trends of the parallels in this procedure were more similar than
what was the case for the first procedure (see Eq. (4.3)). The trend was increasing $|\zeta|$ with respect
to pH.

$$\zeta = -4.79\text{pH} - 55.93 \tag{4.3}$$

4.2.2   Zeta potential as a function of electrolyte concentration

To get a better understanding of how the addition of counter-ions with different valencies affect
the zeta potential of the emulsion, the zeta potential was measured for emulsions containing
varying concentrations of chlorine salts with monovalent sodium (Na^+), divalent calcium (Ca^{2+})
and trivalent ions alumina (Al^{3+}) and iron (Fe^{3+}) as cations.

Sodium chloride

The addition of low concentration sodium chloride seemed to have no significant impact on the
zeta potential, as can be seen in Fig. 4.5a).

When the NaCl concentration was elevated $(C_{\text{NaCl}} > 0.01 \, \text{mol} \, \text{l}^{-1})$, the absolute value of the zeta
potential increased approximately logarithmic as shown in Fig. 4.5b). Logarithmic regression
yielded a statistical model of the zeta potential as a function of salt concentration. Regression of
$C_{\text{NaCl}} > 0.01 \, \text{mol} \, \text{l}^{-1}$ resulted in Eq. (4.4).

It should also be noted that material degradation of the electrodes in the zeta sizer cuvette was
observed at high salt concentration, seen as a change in colour from shiny golden metal to black.
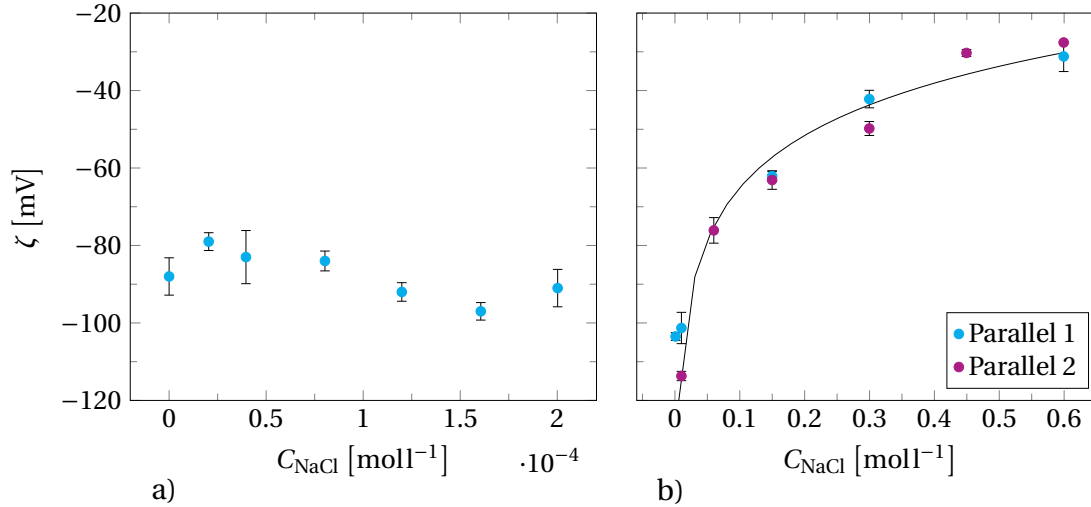
$$\zeta = 19.48 \ln C_{\text{NaCl}} - 20.24 \tag{4.4}$$

Figure 4.5: Zeta potential, ζ, as a function of sodium chloride concentration, C_{NaCl}. pH $= 8.0 \pm 0.2$. a) Low salt concentrations; b) High salt concentrations

Calcium chloride

The effect of adding $CaCl_2$, with divalent cation, was studied by measuring the zeta potential as a function of electrolyte concentration, and the resulting data are plotted in Fig. 4.6a). It was observed that the magnitude of the zeta potential initially decreased at a quite steep slope as a function of $CaCl_2$ concentration, quantified by Eq. (4.5). When the concentration exceeded $30\,\mu\text{mol}\,l^{-1}$, the curve flattened, and the zeta potential seemed to be unaffected by further calcium addition. The results from higher concentrations, however, indicated a further logarithmic decrease in the zeta potential magnitude with respect to $CaCl_2$ concentration, as illustrated in Fig. 4.6b) and quantified by Eq. (4.6).

$$\zeta = 1.34 C_{\text{CaCl}_2} - 86.88 \tag{4.5}$$
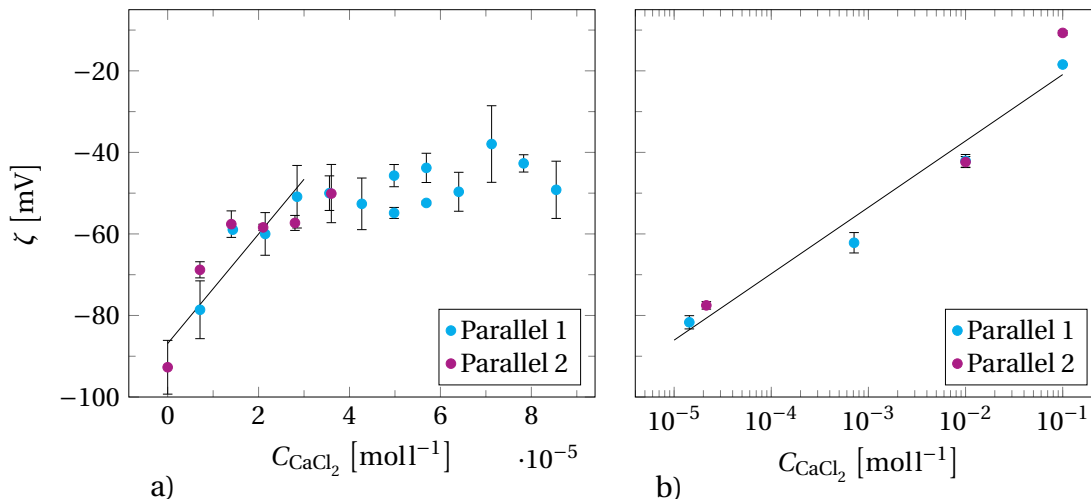
$$\zeta = 7.07 \ln C_{\text{CaCl}_2} - 4.63 \tag{4.6}$$

Figure 4.6: Zeta potential, ζ, as a function of calcium chloride concentration, C_{CaCl_2}. pH = 8.0 ± 0.2. a) Low concentrations; b) High concentrations

Aluminium chloride

The zeta potential as a function of electrolyte concentration is plotted in Fig. 4.7a). Addition of aluminium chloride seemed to have no effect on the zeta potential. At $AlCl_3$ concentrations of about $10\,\mu moll^{-1}$, the Zetasizer experienced problems with the distribution data. At higher concentrations still, the error bars demonstrate a broad zeta potential distribution. To investigate whether the issues arose from the specific stock solution of $13\,\mu moll^{-1}$, a subsequent run with concentration of $20\,\mu moll^{-1}$ was conducted. The zeta potential magnitude was approximately the same as for lower concentrations, and broad zeta potential distribution data was observed (see Fig. 4.8).

It should also be noted that the addition of NaOH to adjust the pH of the $AlCl_3$ electrolyte emulsions clearly showed an increase in turbidity of the sample with increasing NaOH addition. This was also observed when $FeCl_3$ was added as a substitute for $AlCl_3$.

Iron (III) chloride

Iron(III) chloride, which also has a trivalent cation, was introduced as a substitute to $AlCl_3$. The zeta potential as a function of $FeCl_3$ concentration is plotted in Fig. 4.7b. The first parallel showed a significant increase in zeta potential at quite low concentrations, however the second parallel did not confirm this trend. Broad zeta potential distributions poses an issue for $FeCl_3$ concentrations above $10\,\mu moll^{-1}$. The zeta potential with respect to the ionic strength of $FeCl_3$, $CaCl_2$
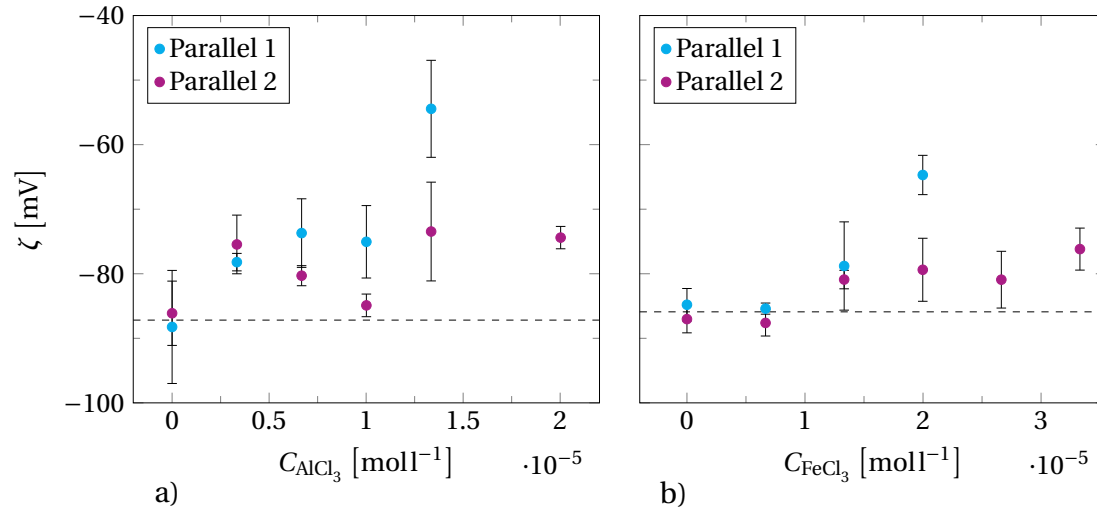
Figure 4.7: Zeta potential, ζ, as a function of salt concentration, C_i, for salt i. The dashed line indicates ζ without electrolyte. a) $i = AlCl_3$; b)$i = FeCl_3$. pH $= 8.0 \pm 0.2$

and NaCl is plotted in Fig. 4.9.

Figure 4.8: Zeta potential distribution of $AlCl_3$ electrolyte emulsion. ζ_a is the apparent zeta potential.

Figure 4.9: Zeta potential (ζ) as a function of ionic strength of the salts (I_i). pH $= 8.0 \pm 0.2$

Figure 4.10: Zeta potential, ζ, as a function of salt concentration, C_i. pH $= 8.0 \pm 0.2$

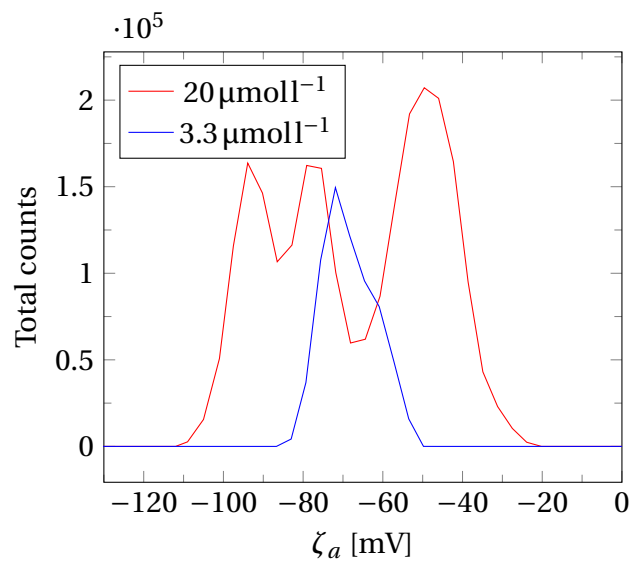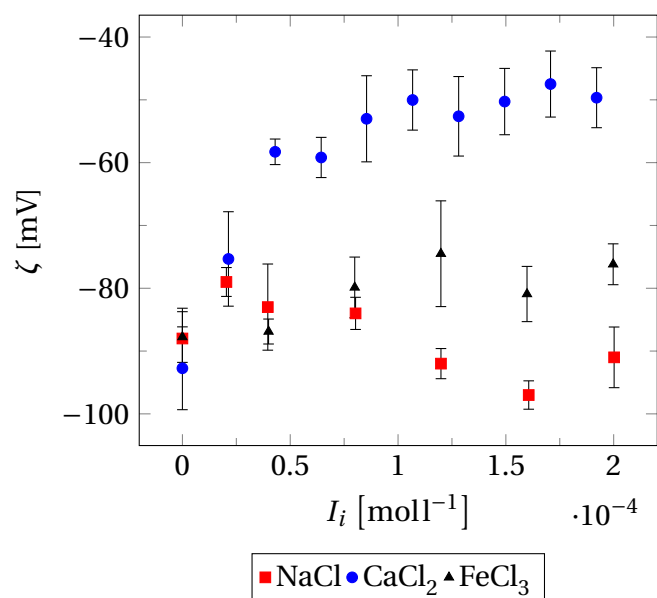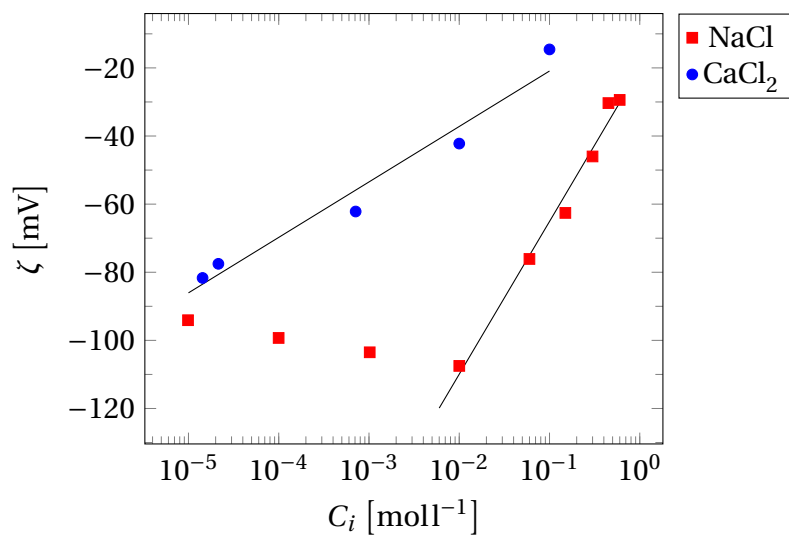## 4.3   Sample convection compensation

A method for determining droplet size distribution as well as water profile of water-in-oil emulsions over time using low-field nuclear magnetic resonance (NMR) was described in Section 2.3.2. A new NMR method needed to be developed in order to analyse oil-in-water emulsions. An issue that arose with having a continuous phase of low viscosity, in this case water, was convection that induced motion of the emulsion sample when inserted into the NMR instrument. As a consequence of this motion, the first measurements made by the NMR had to be rejected; this meant that the method could not be used to study the emulsion immediately after preparation.

To assess the limitations of the NMR method caused by convection, two modification measures were suggested; the sample dimensions could be reduced to increase the critical Rayleigh number, and the effect of this was studied by testing substitutes to the standard NMR tube. In addition, a convection compensating signal sequence was developed. To test these convection compensating signal, the intensity of bulk signal was measured as a function of sample height. All of the measurements were done with a observation time (D5 value) of 1 s unless otherwise is stated. The results of other D5 values are presented in Appendix B.

4.3.1   NMR tube modification

The first part of the investigation considered the effect of using different kinds of NMR sample tubes to reduce the sample dimensions, which in theory should raise the onset barrier of thermal convection in the sample. The water profile obtained from low-field NMR of water in a standard NMR tube was compared to that of a narrower NMR tube, as well as standard NMR tube with a customised teflon quadruple sample divider inserted.

As plotted in Fig. 4.11, the first two runs with the 15 mm tube showed great deviation from the subsequent runs in the same measurement; the intensity had two maxima with a «valley» in between. The 9 mm tube showed an anomaly in the first run that was significantly less distinct than for the corresponding samples in the 15 mm tube. Adding the sample divider resulted in an intensity where the two first runs differed from the rest (see Fig. 4.12), similarly to the results obtained without the divider.

Figure 4.11: Normalised intensity as a function of sample height obtained from low-field NMR before any modifications had been made. The left plot is with a 15 mm tube, the right plot is with a 9 mm tube.

Figure 4.12: Normalised intensity as a function of sample height obtained from low-field NMR before any modifications had been made. The sample was measured in a 15 mm tube containing a teflon quadruple sample divider.

4.3.2   Modified NMR program

The next step of the NMR method improvement was to compensate for convection in the NMR signal sequence. For this part, only the standard NMR tube was used to test the effect of the compensation. Testing the modified sequence, see Fig. 4.13, yielded a fluctuating intensity that declined with respect to height.

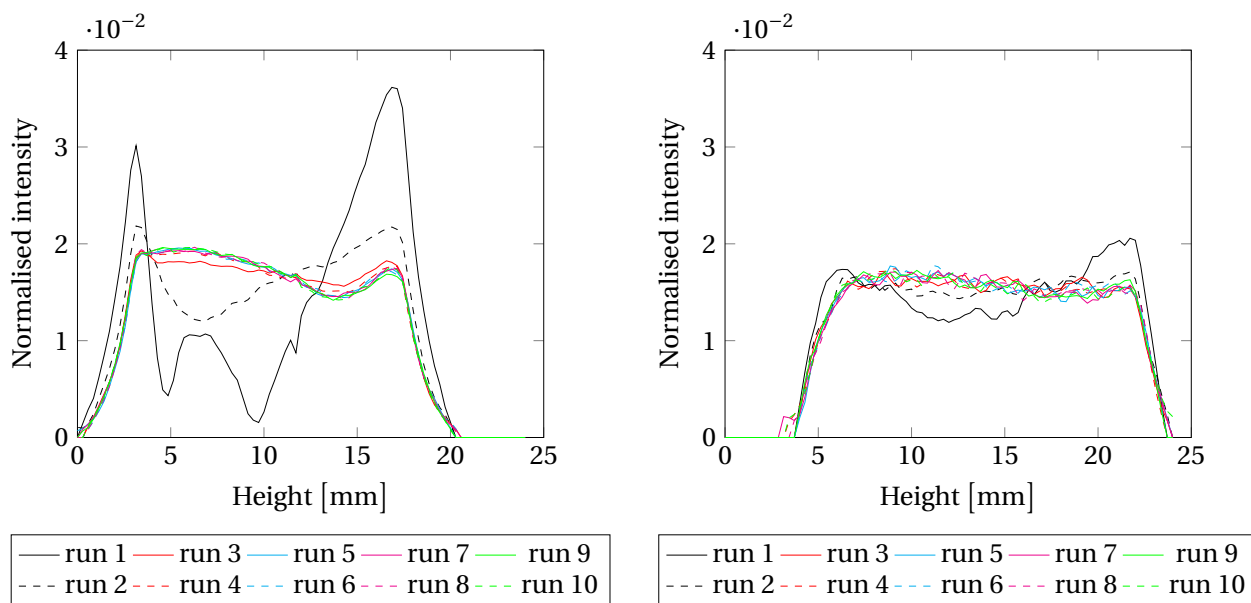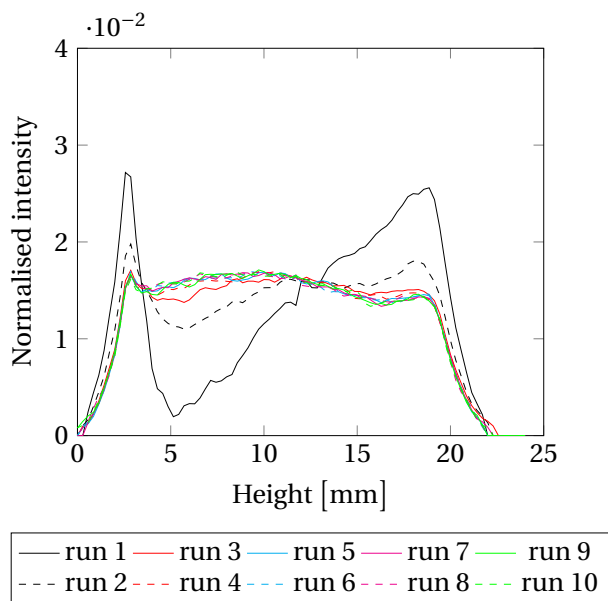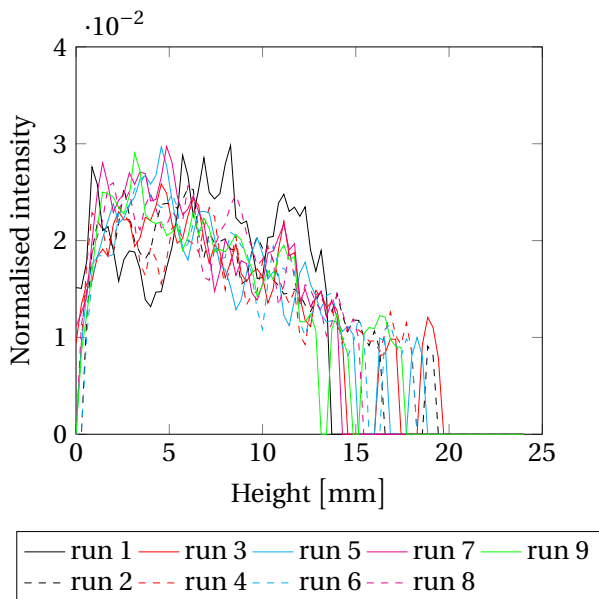**Figure 4.13:** Normalised intensity as a function of sample height obtained from low-field NMR before any modifications had been made. The sample was measured in a 15 mm tube.

4.3.3   Modification with increased number of scans

To study whether or not signal noise was the reason for the fluctuating intensity that resulted from modifying the NMR signal sequence, the number of scans was increased. The result from this alteration is presented in Fig. 4.14. The level of noise seemingly decreased with increasing number of scans. The intensity had a negative slope with increasing height. Some final adjustments were made on the NMR signal sequence that resulted in the relatively smooth results shown in Fig. 4.15.
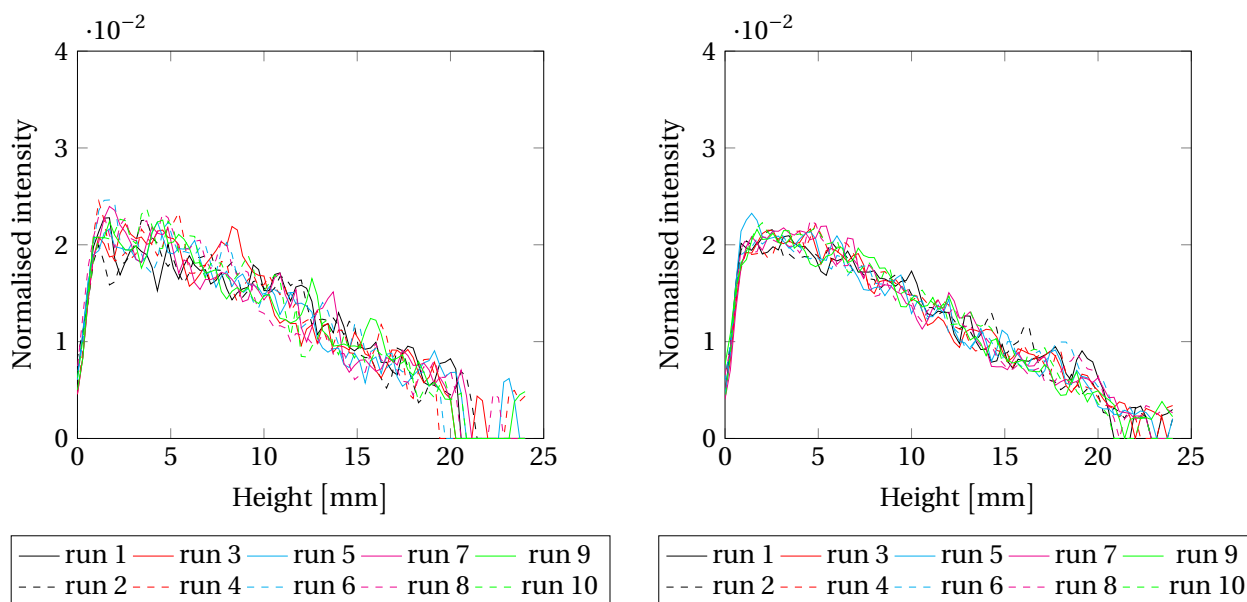
Figure 4.14: Normalised intensity as a function of sample height obtained from low-field NMR with convection compensating sequence and increased number of scans; 8 and 16 scans for the left and right plot, respectively. The sample was measured in a 15 mm tube containing a teflon quadruple sample divider.
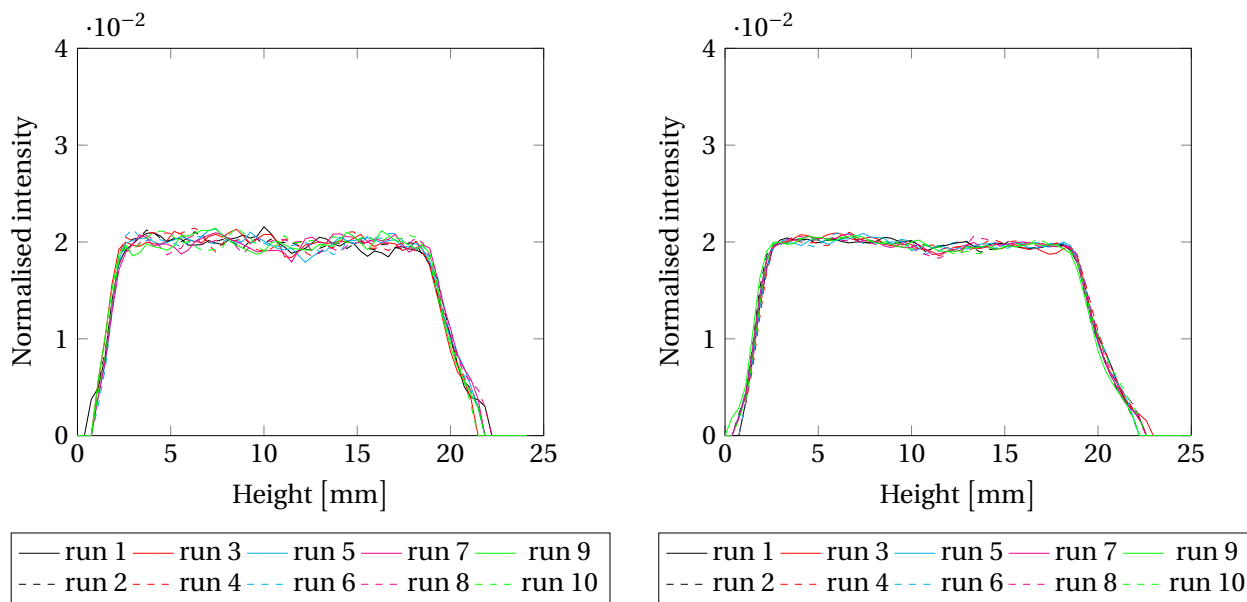

Figure 4.15: Normalised intensity as a function of sample height obtained from low-field NMR with final modifications and 4 scans per run. The samples were measured in a 15 mm tube, with D5 values of 1000 ms for the left sample and 150 ms for the right sample.

5 | Discussion

5.1 Emulsion stability based on preparation parameters

The layers formed in the emulsion seemed to become stationary after a couple of hours, as no evident change was visually observed over time. It may seem as though the emulsion enters a state where the droplets are located according to their size. This also appears from the microscope image, where the droplets in the middle layer are about ten times smaller than the droplets observed after mixing the layers. Hence, it can seem as though the droplets in the middle layer are in a size range where the thermodynamic forces are stronger than the gravitational forces. On the other hand, due to buoyancy, the rate of creaming depends on the size of the creaming particle, which would also leave the droplet sizes in the middle layer smaller than those of the top layer.

Increasing the energy input by increasing the mixing frequency seems to result in better stability. This is probably due to the fact that higher energy input can produce smaller droplets, which are more resistant to creaming as gravitational forces are practically negligible for small particles. This means that thermodynamically favourable spreading of droplets through diffusion is the dominating effect on droplet motion. Emulsions prepared with too low energy input will have a broad droplet size distribution (DSD) and thus be more subject to Ostwald ripening which causes a difference in Laplace pressure and, consequently, Ostwald ripening. The Ostwald ripening will cause some of the droplets to grow into the size range where the force of gravity no longer is negligible, causing the droplets in question to be subject to creaming. The fact that heptane is slightly soluble in water ($0.05\,\mathrm{g\,l^{-1}}$) [31] can also elevate the rate of Ostwald ripeningand thus further reduce the stability of the emulsion. At low mixing frequencies, the applied energy may be too low for the droplet deformation energy to overcome the Laplace pressure and thereby forming droplets.

The amount of emulsifying agent sodium dodecyl sulfate (SDS) may be an explanation for the

43

lack of stability for emulsions prepared at low mixing frequencies; if the surface coverage of SDS on the emulsion droplets is poor, the SDS molecules may polarise when two droplets are approaching each other. The polarisation cause the area of the droplet that is facing the other droplet to become free of surfactants and thus have low if any resistance towards coalescence.

The ability of good emulsifying agents to also work as foaming agents could explain the foaming during emulsion preparation, a theory that is supported by the fact that the use of SDS has been reported as a foaming agent in previous research [33]. Reducing the amount of SDS to reduces the amount of foam produced, but also the stability of the emulsion. The latter can be explained as a reduction of SDS concentration will reduce the surface coverage of the SDS on the droplets, increasing the surface tension and thus reducing the stability of the emulsion droplets. This strongly indicates the presence of a trade-off between the amount of foam produced and emulsion stability. The amount of foam produced also seems to correlate to the mixing frequency. This is probably because an increase in mixing velocity yields an increase in liquid-air contact area, which is a criteria for foaming.

Stable hexadecane-in-water emulsions has been prepared for oil contents higher than 40 % [34], which were stabilised by close packing of droplets. This is not applicable for measurements in the zeta sizer, as the instrument procedure requires a maximum volumetric content of 0.05 % of the dispersed phase.

Decanol was added as a foam inhibitor, but the addition does not seem to reduce the amount of foam produced, which may be due to the low amount of decanol added. The consequence of adding more co-surfactant could be a decrease in emulsion stability, which is why it was not pursued as a solution.

The stock emulsion used for zeta potential analysis seemed to be satisfyingly stable from visual observation, however the characterisation done by the newly developed low-field NMR method Fig. 4.3 showed that a top layer of almost 60 % oil phase was formed immediately after the preparation of the emulsion. The fast creaming rate can be explained by the droplet size distribution (DSD) obtained from the same NMR measurement; a broad DSD with droplet diameters up to 100 µm was observed, and these large droplets will cream fast due to buoyancy. As the microscope image from the middle part of the emulsion shows, the droplets left in the middle are smaller and probably in a size range where both entropy and gravitation has an effect, keeping the creaming rate low.

5.2 Zeta potential

5.2.1 pH

When ζ was measured with varying pH, the trends of the two parallels are quite diverse; the slope of parallel 1 is more than three times that of parallel 2. This could be due to the fact that portions for each run was taken subsequently from the same emulsion at different times. Since significant changes can happen to an emulsion over short time spans, the properties of each dilution may be quite different from the others.

The change in procedure seems to have improved the reproducibility of the experiment, still some of the standard deviations are quite large. The reason for this may be that there is a trade-off between the time spent on preparing the emulsion for the zeta sizer and the change in emulsion properties; if too much time is spent on the preparation an unstable emulsion may have creamed or even coagulated before the measurements begin. On the other hand, the sample requires some time to equilibrate as the pH is adjusted, so if the emulsion is removed from the pH-meter too soon the pH may not be uniformly distributed throughout the sample. Since the zeta sizer only measures ζ for a small portion of the sample, the results obtained from a non-uniform emulsion does not necessarily represent the entire sample.

A common feature of all the measurements can still be observed; the absolute value of the zeta potential, $|\zeta|$, is increasing with increasing pH. This may be due to adsorption of H^+ and OH^- ions in the interface, which neutralises or amplifies the negative charge of the droplet surface, respectively.

As stated by the Schulze-Hardy rule, counter-ions usually have greater impact on ζ than co-ions, which is confirmed by the declining slope of the ζ as a function of pH, keeping in mind that pH is the negative logarithm of hydrogen concentration.

5.2.2 Influence of electrolyte concentration

In the context of emulsion stability theory, the addition of counter-ions reduces the maximum potential energy, so that coagulation is more accessible.

NaCl

A slight increase in the absolute value of the zeta potential was observed with increasing NaCl electrolyte concentration at low concentrations. This phenomenon has been observed in previous studies of oil-in-water emulsions [5, 21], and could be due to the adsorption of chloride ions on the oil droplet surface leading to an increase in negative charge. The zeta potential seems to reach a minimum as the effect of the compression of the electrical double layer by the positively charged sodium ions exceed the effect of the Cl^- adsorption.

The absolute value of the zeta potential starts to decrease as the electrolyte concentration is further increased. This result is expected, as addition of counter-ions generally leads to a compression of the electrical double layer and a corresponding reduction in $|\zeta|$.

CaCl$_2$

The steep decline of $|\zeta|$ that is observed at low concentrations of calcium chloride electrolyte indicates that the divalent calcium ions to have a strong effect on the zeta potential. When comparing the ζ for $CaCl_2$ and NaCl electrolyte concentrations, it can be observed that the addition of $CaCl_2$ affects the ζ at much lower electrolyte concentrations than what is the case for NaCl; $|\zeta|$ has been reduced to less than $-80\,mV$ at a $CaCl_2$ concentration of $7.1\,\mu mol\,l^{-1}$, whereas the NaCl concentration required to reduce $|\zeta|$ to the same magnitude was as high as $60\,mmol\,l^{-1}$. That is a ratio of more than 8000. It may seem as though the effect of Cl^- ions believed to adsorb to the surface more strongly than Na^+ is negligible compared to the neutralising effect of Ca^{2+} ions. Calcium ions also have a low degree of hydration in aqueous solution, making them even more prone to adsorb to negatively charged species than those of high degree of hydration [6].

FeCl$_3$ and AlCl$_3$

The zeta potential seems to have roughly no variation with increasing concentration of either of the two trivalent chloride salts, $AlCl_3$ and $FeCl_3$, in the investigated range of concentrations. Due to too broad distribution data of samples with $C_{AlCl_3} > 10\,\mu mol\,L^{-1}$, zeta potential measurements were only done for lower concentrations of $AlCl_3$.

According to the Schulze-Hardy rule, $CCC \propto z^{-6}$, so an electrolyte with a trivalent counterion should in theory lower the critical coagulation concentration considerably due to compression of the electrostatic double layer. This should especially be observed when comparing the effect

of electrolytes with counter-ions of different valency. The lack of influence of $FeCl_3$ and $AlCl_3$ on the zeta potential in this experiment therefore needs to be explained by factors other than DLVO theory.

One possible explanation for the deviation from theory is that the effect of $FeCl_3$ is so fast that coagulation and subsequent creaming occurs before the ζ measurements are conducted. If the majority of droplets have floated to the top of the sample before the measurement starts, they will not be accounted for in the small portion of the sample the zeta sizer includes in the measurement. In that case, the measurement data are not representative for the entire sample. By evaluating the oil profile of the stock emulsion obtained from low-field NMR, it was observed that a dense layer of up to 60 % hexadecane formed instantaneously after the emulsion had been prepared; this further supports the idea that the emulsion is non-uniform.

Both $AlCl_3$ and $FeCl_3$ are corrosive in contact with metals, so it is a possibility that the zeta sizer cuvette electrodes are degraded by the salt, resulting in poor measurement quality.

The deviation between the parallels can probably be explained by the difficulty of achieving the correct pH due to the trade-off between emulsion stability and sample preparation time.

Iron (III) hydroxide is listed as practically insoluble in water, and since the concentration of hydroxide ions increase with increasing pH it is a possibility that the iron ions precipitate as $Fe(OH)_3$ at the current pH. Such precipitation could also be an explanation for the change in turbidity when adding NaOH to the emulsion for pH adjustments. Alternatively, the change in turbidity may be due to droplet coagulation and change in droplet sizes. In that case, the Tyndall effect of colloidal dispersions would be the explanation.

5.3 Sample convection

The effect of sample convection was more visible with increasing D5. In this sense, carrying out the self-diffusion experiment at elevated D5 values emphasises the disruptions caused by convection, as well as the effect of the convection compensating measures.

In the results measured before any modifications had been made on the low-field NMR program, a valley was detected in the first two runs (Fig. 4.11). This is obviously not correct, given as the sample is pure water so the content is the same throughout the entire height of the sample. The proposed reason for the minimum is that it is caused by Rayleigh-Bénard convection in the sample. Since the sample may be subjected to heating from below when it is inserted to the

instrument, giving rise to a temperature gradient. The relatively low viscosity of water compared to previously examined systems [35, 8] may cause a Rayleigh number that exceeds the critical value resulting in convection. The convection seems to disrupt the first diffusion measurements, after which the system seems to become stationary.

In general, the samples measured in the narrow tube seems to be less affected by convection than the samples measured in the standard NMR tubes. Reducing the sample dimensions by using a narrower NMR tube should in theory reduce the Rayleigh number. If the Rayleigh number becomes lower than the critical Rayleigh number, fluid motion caused by convection will cease to occur. This is a great advantage, however practical issues arise from having to use a tube that does not fit properly into the instrument; fitting the 9 mm tube into the instrument is time consuming, which is not ideal when studying a possibly kinetically unstable system.

The standard NMR tube provided similar results with and without the sample divider, so it seems as if introducing the sample divider had little if any effect on the Rayleigh number.

Introducing the convection compensating sequence seems to reduce the effect of convection, however, the noise in the resulting intensity makes it hard to draw any conclusions. Increasing the number of scans seems to reduce the noise, but the downward-sloping profile (Fig. 4.14) indicates that further modifications needs to be made. A final modification conducted seems to implement the convection compensating sequence in a way that minimises fluctuation as well as the deviation between the runs.

6 | Conclusion

O/W emulsions were prepared and layers of different turbidity were visually observed. The creaming rate decreased with increasing oil phase density, mixing frequency and mixing time, whereas the foam generated during emulsion preparation was reduced by lowering the surfactant amount, mixing frequency and mixing time.

A combination of parameters that produced an adequately stable emulsion was used to prepare emulsions for emulsion stability investigation by zeta potential measurements. The effect of varying pH on the zeta potential of the emulsion was increasing absolute value of zeta potential, and thus increasing stability, with increasing pH. The effect of electrolyte concentration on emulsion stability depends on the valency of the droplet surface charge counter ion. Addition of the divalent Ca^{2+} ions through $CaCl_2$ reduced the absolute value of the zeta potential at distinctively lower concentrations than the addition of Na^+ through NaCl. These results suggests that emulsion stability decreases with increasing electrolyte concentration and that the destabilising effect gets stronger for increasing valency of the electrolyte counter-ions. The same effect was not observed when adding trivalent ions, which was unexpected and suggests that the success of the procedure depends on the stability of the initial emulsion.

The NMR experiments performed to eliminate the disturbances on diffusion measurements caused by thermal convection was successfully conducted. The new NMR program developed by the supplier, Antek AS, was proven to work well for oil-in-water emulsions.

7 | Further research

By optimising the surfactant amount to ensure maximum surface coverage, better emulsion stability should be attainable. An emulsion used for similar stability studies as in this project should be stable enough to resist creaming for at least 15 min to allow for destabilisation to be observable. Further it should not be so stable that it can not be destabilised within reasonable time limits.

Using the low-field NMR procedure tested in this project, an optimised emulsion could be analysed quantitatively over time. By adding salts with cations of different valencies, the influence of electrolyte concentration and valency on emulsion stability can be measured of the entire sample. The droplet size distribution combined with oil profile obtained from low-field NMR can give an indication of the rate of creaming and/or coalescence.

It is also possible to investigate the emulsion behaviour in porous solid media similar to the rock formations in an oil reservoir in situ by using the program developed in this project. The study of emulsion behaviour in porous plugs is an ongoing project at the Ugelstad laboratory [36].

Bibliography

[1] Bernard Gilland. Population, economic growth, and energy demand, 1985-2020. *Population and Development Review*, 14(2):pp. 233–244, 1988.

[2] Vladimir Alvarado and Eduardo Manrique. Enhanced oil recovery: An update review. *Energies*, 3(9):1529–1575, 2010.

[3] L.L. Schramm and Petroleum Recovery Institute. *Emulsions: Fundamentals and Applications in the Petroleum Industry*. Advances in Chemistry Series. American Chemical Society, 1992.

[4] Tor Austad, Alireza RezaeiDoust, Tina Puntervold, et al. Chemical mechanism of low salinity water flooding in sandstone reservoirs. In *SPE improved oil recovery symposium*. Society of Petroleum Engineers, 2010.

[5] G. Rios, C. Pazos, and J. Coca. Zeta Potentials of Cutting-Oil Water Emulsions: Influence of Inorganic Salts. *Journal of Dispersion Science and Technology*, 19(5):661–678, 1998.

[6] M.L Jayme, D.E Dunstan, and M.L Gee. Zeta potentials of gum arabic stabilised oil in water emulsions. *Food Hydrocolloids*, 13(6):459–465, 1999.

[7] B. P. Binks, W. G. Cho, P. D I Fletcher, and D. N. Petsev. Stability of oil-in-water emulsions in a low interfacial tension system. *Langmuir*, 16(9):1025–1034, 2000.

[8] NVDT Opedal, G Sørland, and J Sjöblom. Methods for droplet size distribution determination of water-inoil emulsions using low-field nmr. *Diffusion Fundamentals*, 9(7):1–29, 2009.

[9] Sunil Lalchand Kokal et al. Crude oil emulsions: A state-of-the-art review. *SPE Production & facilities*, 20(01):5–13, 2005.

[10] Preben C. Mørk. *Overflate og kolloidkjemi : Grunnleggende prinsipper og teorier*. Department for Chemical Engineering, NTNU, 8 edition, 2004.

[11] Johan Sjöblom. *Emulsions and Emulsion Stability : Surfactant Science Series.* CRC Press, 2 edition, 2006.

[12] Paul Becher. *Encyclopedia of emulsion technology*, volume 1. New York : Dekker, 1983.

[13] B Abismaïl, J.P Canselier, A.M Wilhelm, H Delmas, and C Gourdon. Emulsification by ultrasound: drop size distribution and stability. *Ultrasonics Sonochemistry*, 6(1–2):75 – 83, 1999.

[14] Tharwat Tadros. Coalescence. In Tharwat Tadros, editor, *Encyclopedia of Colloid and Interface Science*, pages 84–84. Springer Berlin Heidelberg, 2013.

[15] D.J. Shaw. *Introduction to Colloid and Surface Chemistry*. Chemical, Petrochemical & Process. Butterworth-Heinemann, 1992.

[16] Wilder D Bancroft. The theory of emulsification, v. *The Journal of Physical Chemistry*, 17(6):501–519, 1913.

[17] Andrew P Sullivan and Peter K Kilpatrick. The effects of inorganic solid particles on water and crude oil emulsion stability. *Industrial & engineering chemistry research*, 41(14):3389–3404, 2002.

[18] Robert J. Hunter. *Zeta Potential in Colloid Science: Principles and Applications*. Colloid science. Academic Press, 1981.

[19] P.C. Hiemenz and R. Rajagopalan. *Principles of Colloid and Surface Chemistry, Third Edition, Revised and Expanded*. Undergraduate Chemistry: A Series of Textbooks. Taylor & Francis, 1997.

[20] Malvern Instruments Ltd. *Zetasizer Nano Series User Manual*, 2003.

[21] EE Isaacs and RS Chow. Practical aspects of emulsion stability. *Advances in Chemistry Series*, (231):51–77, 1992.

[22] P. Atkins and J. de Paula. *Atkins' Physical Chemistry*. OUP Oxford, 2010.

[23] M. Helbæk and S. Kjelstrup. *Fysikalsk kjemi*. Fagbokforl., 2006.

[24] John S. Eow, Mojtaba Ghadiri, Adel O. Sharif, and Trevor J. Williams. Electrostatic enhancement of coalescence of water droplets in oil: a review of the current understanding. *Chemical Engineering Journal*, 84(3):173 – 192, 2001.

[25] Stoyan I. Karakashev and Michaela V. Grozdanova. Foams and antifoams. *Advances in Colloid and Interface Science*, 176–177(0):1 – 17, 2012.

[26] Jan Ketil Solberg. Lysmikroskopi. Department of Materials Science and Eningeering, NTNU, 2011.

[27] Eric Betzig and Jay K. Trautman. Near-field optics: Microscopy, spectroscopy, and surface modification beyond the diffraction limit. *Science*, 257(5067):189–195, 1992.

[28] Sébastien Simon, Xavier Pierrard, Johan Sjöblom, and Geir H. Sørland. Separation profile of model water-in-oil emulsions followed by nuclear magnetic resonance (nmr) measurements: Application range and comparison with a multiple-light scattering based apparatus. *Journal of Colloid and Interface Science*, 356(1):352 – 361, 2011.

[29] Geir Humborstad Sørland. *Dynamic Pulsed-field-gradient NMR*. Springer, 2014.

[30] R Byron Bird, Warren E Stewart, and Edwin N Lightfoot. *Transport phenomena*. John Wiley & Sons, 2007.

[31] Gordon Aylward and Tristan Findlay. *SI Chemical Data*. John Wiley & Sons Australia, Ltd, 42 McDougall Street, milton, Qld 4164, 6 edition, 2008.

[32] Selwyn J. Rehfeld. Adsorption of sodium dodecyl sulfate at various hydrocarbon-water interfaces. *The Journal of Physical Chemistry*, 71(3):738–745, 1967.

[33] Stig E Friberg, Irena Blute, and Per Stenius. Foam stability in a glycerol system. *Journal of Colloid and Interface Science*, 127(2):573 – 582, 1989.

[34] Ratjika Chanamai and D Julian McClements. Creaming stability of flocculated monodisperse oil-in-water emulsions. *Journal of Colloid and Interface Science*, 225(1):214–218, 2000.

[35] Trine Nisja. Filtration of emulsions. Specialization project, Norwegian University of Science and Technology, 2014.

[36] Camilla I. Dagsgård, Trine Nisja, May Grete Sætran, Geir Humborstad Sørland, and Johan Sjöblom. Filtration of emulsions part 1. 2014.

A | Zeta potential data

Average zeta potential, ζ, measured as a function of either pH or electrolyte concentration is shown in the tables of this appendix.

Table A.1: Zeta potential, ζ, with standard deviation, σ, at different pH values for hexadecane-in-water emulsions with sodium dodecyl sulphate as emulsifier.

	Parallel 1			Parallel 2	
pH	ζ [mV]	σ [mV]	pH	ζ [mV]	σ [mV]
2.2	-25.3	4.6	2.2	-60.3	1.9
4.1	-29.7	8.5	4.0	-64.1	0.4
6.1	-73.6	4.4	6.1	-71.6	0.8
8.0	-83.0	1.7	8.0	-73.0	3.7
9.9	-94.2	5.9	10.0	-82.6	3.1

Table A.2: Zeta potential, ζ, with standard deviation, σ, at different pH values for hexadecane-in-water emulsions with sodium dodecyl sulphate as emulsifier.

	Parallel 1			Parallel 2	
pH	ζ [mV]	σ [mV]	pH	ζ [mV]	σ [mV]
2.1	-57.9	5.4	2.2	-83.3	5.8
4.0	-71.3	2.6	4.1	-80.3	3.5
6.1	-85.4	4.4	6.1	-68.4	6.1
8.0	-82.8	1.4	8.0	-100.3	8.8
9.9	-104.3	6.9	10.0	-115.0	1.6

Table A.3: Zeta potential (ζ) with standard deviation (σ) at varying sodium chloride concentrations C_{NaCl} for hexadecane-in-water emulsions with sodium dodecyl sulphate as emulsifier.

C_{NaCl} $[\mu\text{mol}\,\text{l}^{-1}]$	ζ $[\text{mV}]$	σ $[\text{mV}]$
0.0	-88.1	4.8
20.4	-79.2	2.3
39.6	-82.7	6.9
80.3	-83.8	2.6
119.9	-92.0	2.4
160.6	-97.0	2.3
200.2	-91.2	4.8

Table A.4: Zeta potential (ζ) with standard deviation (σ) at varying sodium chloride concentrations C_{NaCl} for hexadecane-in-water emulsions with sodium dodecyl sulphate as emulsifier.

Parallel 1			Parallel 2		
C_{NaCl} $[\text{mol}\,\text{l}^{-1}]$	ζ $[\text{mV}]$	σ $[\text{mV}]$	C_{NaCl} $[\text{mol}\,\text{l}^{-1}]$	ζ $[\text{mV}]$	σ $[\text{mV}]$
0.0	-96.0	5.3	9.0×10^{-7}	-98.4	1.3
9.0×10^{-5}	-90.2	2.3	1.0×10^{-4}	-102.2	3.7
1.0×10^{-5}	-94.1	10.3	1.0×10^{-2}	-113.7	1.2
1.0×10^{-4}	-96.4	6.5	6.0×10^{-2}	-76.1	3.3
1.0×10^{-3}	-103.5	1.0	1.5×10^{-1}	-63.1	2.4
1.0×10^{-2}	-101.3	4.0	3.0×10^{-1}	-49.8	1.8
1.5×10^{-1}	-62.1	1.2	4.5×10^{-1}	-30.3	0.9
3.0×10^{-1}	-42.2	2.3	6.0×10^{-1}	-27.2	0.2
6.0×10^{-1}	-31.2	3.9			

Table A.5: Zeta potential (ζ) with standard deviation (σ) at varying calcium chloride concentrations C_{CaCl_2} for hexadecane-in-water emulsions with sodium dodecyl sulphate as emulsifier.

Parallel 1				Parallel 2			
C_{CaCl_2} $[\mu moll^{-1}]$	I_{CaCl_2} $[\mu moll^{-1}]$	ζ $[mV]$	σ $[mV]$	C_{CaCl_2} $[\mu moll^{-1}]$	I_{CaCl_2} $[\mu moll^{-1}]$	ζ $[mV]$	σ $[mV]$
7.1	21.3	-78.6	7.1	0.0	0.0	-92.7	6.6
14.3	43.0	-59.0	0.1	7.1	21.3	-68.8	2.0
21.5	64.4	-60.0	5.2	14.3	43.0	-57.6	3.3
28.5	85.4	-50.9	7.7	21.5	64.4	-58.4	0.8
35.6	106.8	-50.0	4.2	28.5	85.4	-57.3	1.8
42.7	128.1	-52.6	6.3	35.6	106.8	-50.1	7.1
49.8	149.4	-45.7	2.7				
56.9	170.7	-43.8	3.6				
49.8	149.4	-54.8	1.3				
56.9	170.7	-52.4	0.5				
64.0	192.1	-49.7	4.8				
71.3	213.8	-38.0	9.4				
78.3	234.9	-42.7	2.1				
85.5	256.4	-49.2	7.0				

Table A.6: Zeta potential (ζ) with standard deviation (σ) at varying calcium chloride concentrations C_{CaCl_2} for hexadecane-in-water emulsions with sodium dodecyl sulphate as emulsifier.

Parallel 1				Parallel 2			
C_{CaCl_2} $[moll^{-1}]$	I_{CaCl_2} $[moll^{-1}]$	ζ $[mV]$	σ $[mV]$	C_{CaCl_2} $[moll^{-1}]$	I_{CaCl_2} $[moll^{-1}]$	ζ $[mV]$	σ $[mV]$
0.0	0.0	-90.9	1.4	0.0	0.0	-92.0	2.1
1.4×10^{-5}	4.3×10^{-5}	-81.7	1.6	2.1×10^{-5}	6.4×10^{-5}	-77.5	0.9
7.1×10^{-4}	2.1×10^{-3}	-62.2	2.5	2.1×10^{-5}	6.4×10^{-5}	-77.5	0.9
1.0×10^{-2}	3.0×10^{-2}	-42.1	1.6	1.0×10^{-2}	3.0×10^{-2}	-42.4	1.4
1.0×10^{-1}	3.0×10^{-1}	-18.5	0.1	1.0×10^{-1}	3.0×10^{-1}	-10.7	0.6

Table A.7: Zeta potential (ζ) with standard deviation (σ) at varying aluminium chloride concentrations C_{AlCl_3} for hexadecane-in-water emulsions with sodium dodecyl sulphate as emulsifier.

Parallel 1				Parallel 2			
C_{AlCl_3} $[\mu\text{mol}\,\text{l}^{-1}]$	I_{AlCl_3} $[\mu\text{mol}\,\text{l}^{-1}]$	ζ $[\text{mV}]$	σ $[\text{mV}]$	C_{AlCl_3} $[\mu\text{mol}\,\text{l}^{-1}]$	I_{AlCl_3} $[\mu\text{mol}\,\text{l}^{-1}]$	ζ $[\text{mV}]$	σ $[\text{mV}]$
0.0	0.0	-91.1	8.6	0.0	0.0	-86.1	5.0
3.3	19.8	-78.3	1.7	3.3	19.8	-75.6	5.7
6.7	39.9	-73.7	5.3	6.7	39.9	-82.5	4.6
10.1	60.3	-71.9	4.9	10.1	60.3	-84.7	1.9
13.4	80.1	-54.5	7.5	13.4	80.1	-72.3	5.4
				20.0	120.2	-73.4	0.0

Table A.8: Zeta potential (ζ) with standard deviation (σ) at varying iron(III) chloride concentrations C_{FeCl_3} for hexadecane-in-water emulsions with sodium dodecyl sulphate as emulsifier.

Parallel 1				Parallel 2			
C_{FeCl_3} $[\mu\text{mol}\,\text{l}^{-1}]$	I_{FeCl_3} $[\mu\text{mol}\,\text{l}^{-1}]$	ζ $[\text{mV}]$	σ $[\text{mV}]$	C_{FeCl_3} $[\mu\text{mol}\,\text{l}^{-1}]$	I_{FeCl_3} $[\mu\text{mol}\,\text{l}^{-1}]$	ζ $[\text{mV}]$	σ $[\text{mV}]$
0.0	0.0	-84.8	2.5	0.0	0.0	-87.0	2.1
6.7	40.0	-85.4	0.9	6.7	40.0	-87.6	2.0
13.3	79.9	-78.8	6.8	13.3	79.9	-80.9	1.4
20.0	119.9	-64.7	3.0	20.0	119.9	-79.4	4.9
0.0	0.0	-93.7	2.6	26.6	159.8	-80.9	4.4
				33.3	199.8	-76.2	3.3

B | Sample convection compensation results

The water profile intensity for a sample containing Milli-Q water was measured in a variety of NMR tubes: 9 mm NMR tube (narrow tube), 15 mm NMR tube (standard tube) and standard NMR tube with a teflon quadruple sample divider inserted (see Figs. B.1 to B.8)

Further, a convection compensating NMR sequence was added to suppress the diffusion measurement disturbances caused by Rayleigh-Bénard convection. The effect of the applied sequence can be seen from Figs. B.9 and B.10.

To reduce the amount of noise in the measurements, the number of scans for each run was increased from 4 in the preceding measurements to 8 and 16, respectively. The resulting normalised intensities were plotted with respect to sample heigh in Figs. B.11 and B.12.

B.1   Modification of sample dimensions
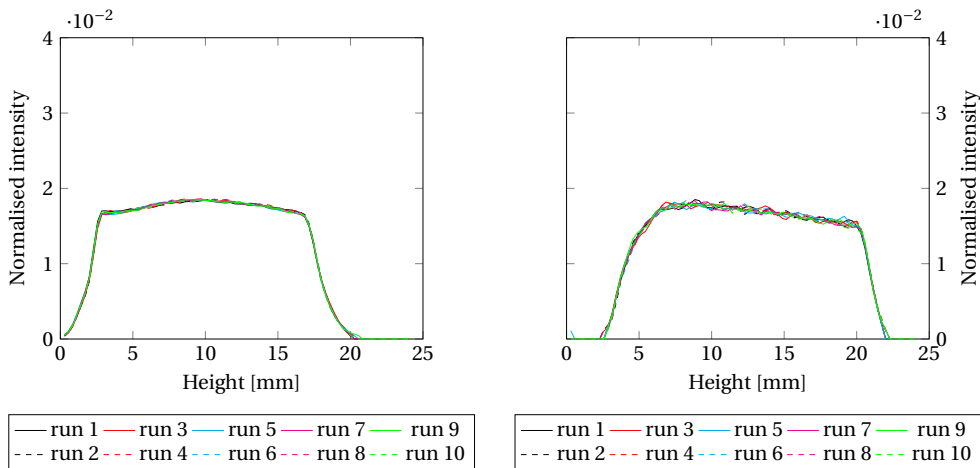
Figure B.1: Normalised intensity as a function of sample height obtained from low-field NMR before modifications with D5 = 50 ms. Left plot: 15 mm tube; right plot: 9 mm tube.
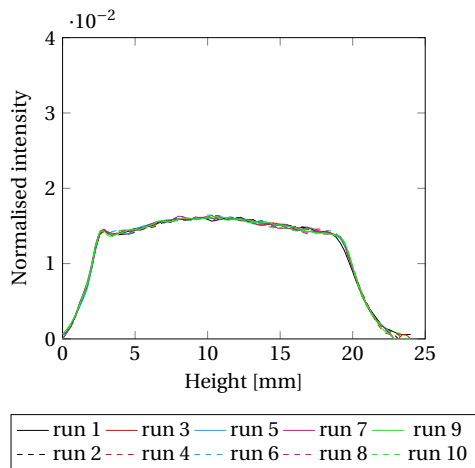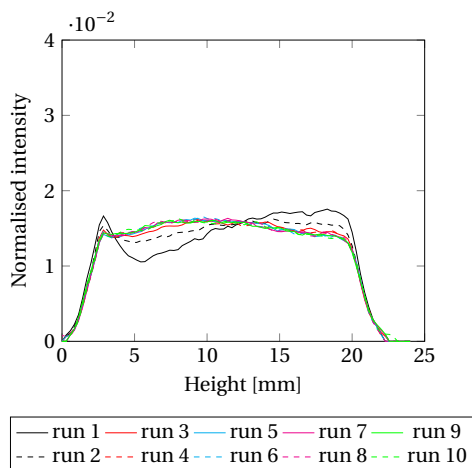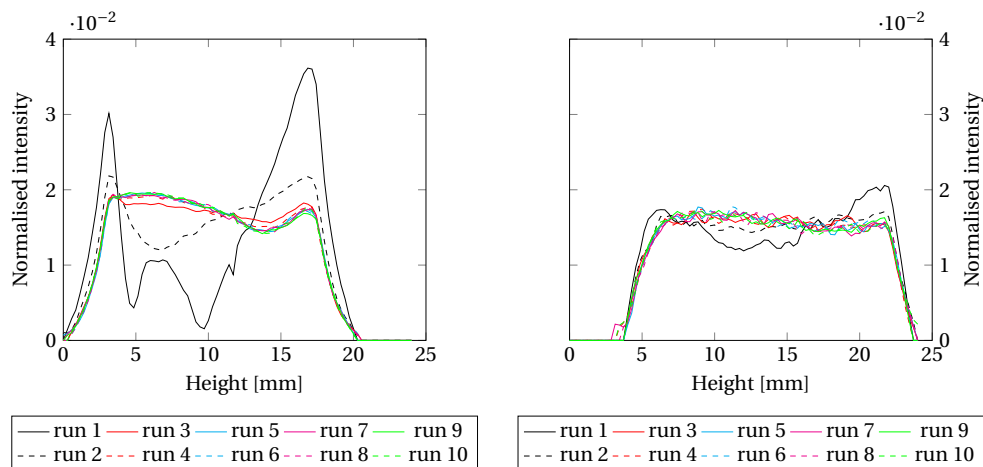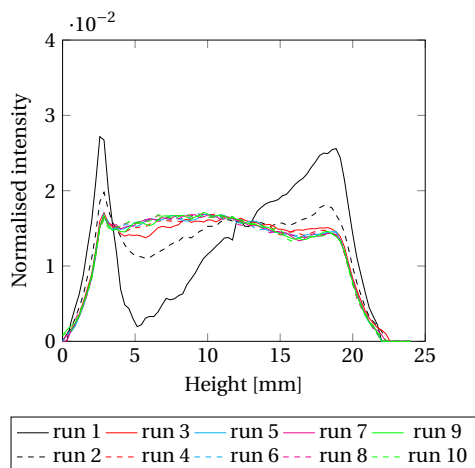

Figure B.2: Normalised intensity as a function of sample height obtained from low-field NMR before any modifications had been made with D5 = 50 ms. Measured in 15 mm tube containing a teflon quadruple sample divider.
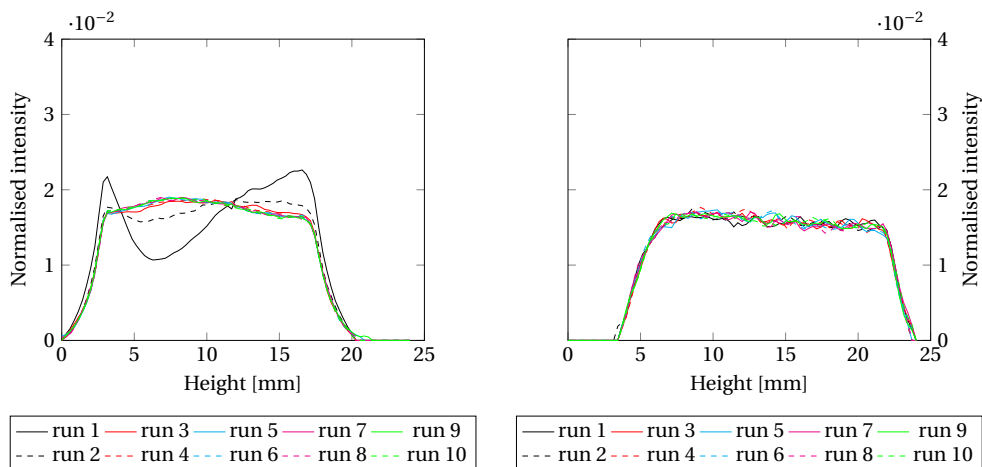
Figure B.3: Normalised intensity as a function of sample height obtained from low-field NMR before modifications with D5 = D5 = 500 ms. Left plot: 15 mm tube; right plot: 9 mm tube.

Figure B.4: Normalised intensity as a function of sample height obtained from low-field NMR before modifications with D5 = D5 = 500 ms. Measured in 15 mm tube containing a teflon quadruple sample divider.
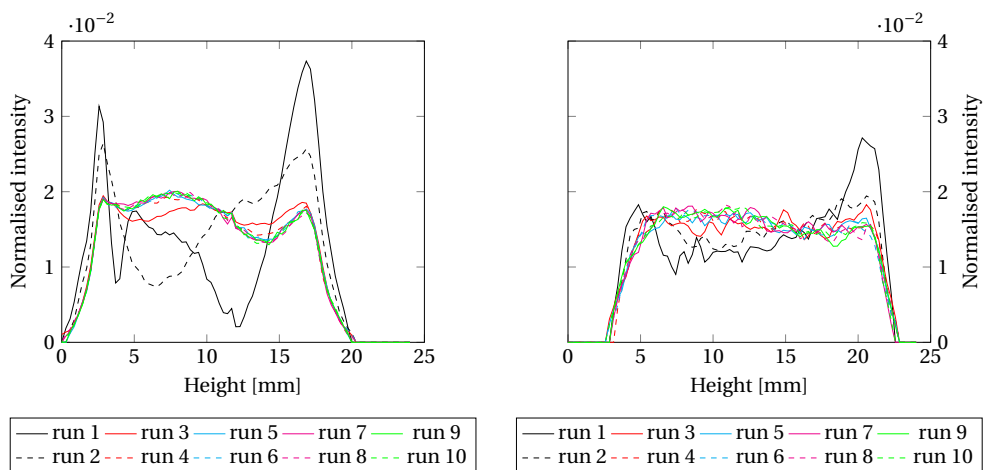
Figure B.5: Normalised intensity as a function of sample height obtained from low-field NMR before modifications with D5 = D5 = 1 s. Left plot: 15 mm tube; right plot: 9 mm tube.
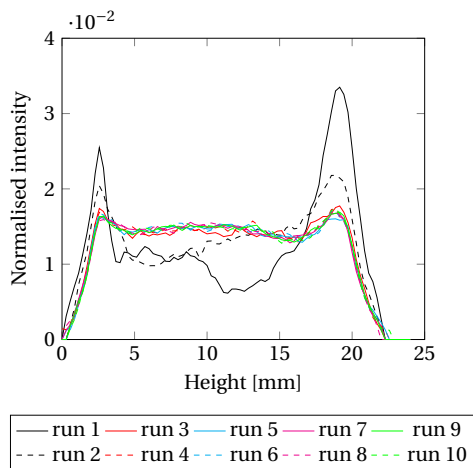

Figure B.6: Normalised intensity as a function of sample height obtained from low-field NMR before modifications with D5 = D5 = 1 s. Measured in 15 mm tube containing a teflon quadruple sample divider.

Figure B.7: Normalised intensity as a function of sample height obtained from low-field NMR before modifications with D5 = 1.5 s. Left plot: 15 mm tube; right plot: 9 mm tube.

Figure B.8: Normalised intensity as a function of sample height obtained from low-field NMR before modifications with D5 = 1.5 s. Measured in 15 mm tube containing a teflon quadruple sample divider.
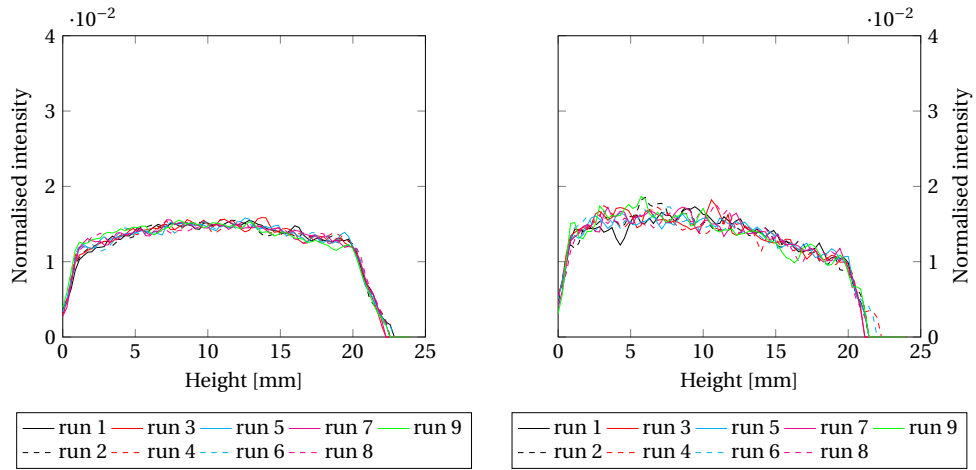
B.2   Modification of NMR program

Figure B.9: Normalised intensity as a function of sample height obtained from low-field NMR after program modifications measured in 15 mm tube. Left plot: $D5 = 250$ ms; right plot: $D5 = 500$ ms.
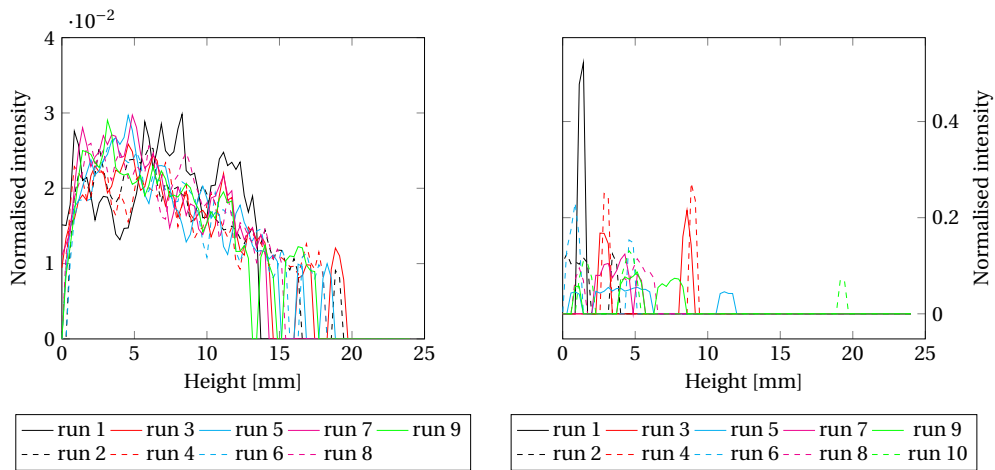

Figure B.10: Normalised intensity as a function of sample height obtained from low-field NMR after program modifications measured in 15 mm tube. Left plot: $D5 = 1$ s; right plot: $D5 = 1.5$ s.
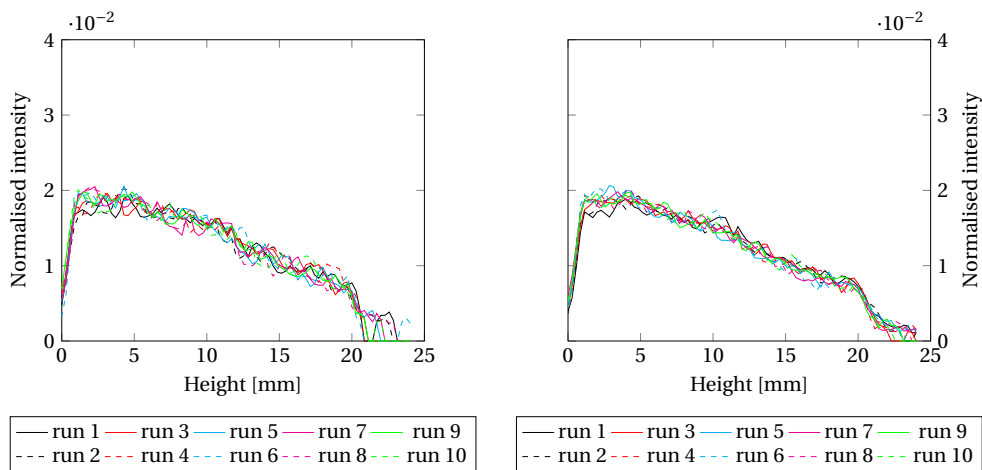
B.3   Modification with increased number of scans

Figure B.11: Normalised intensity as a function of sample height obtained from low-field NMR after program modifications measured in 15 mm tube with $D5$ = 750 ms with varying number of scans (ns). Left plot: ns = 8; right plot: ns = 16.
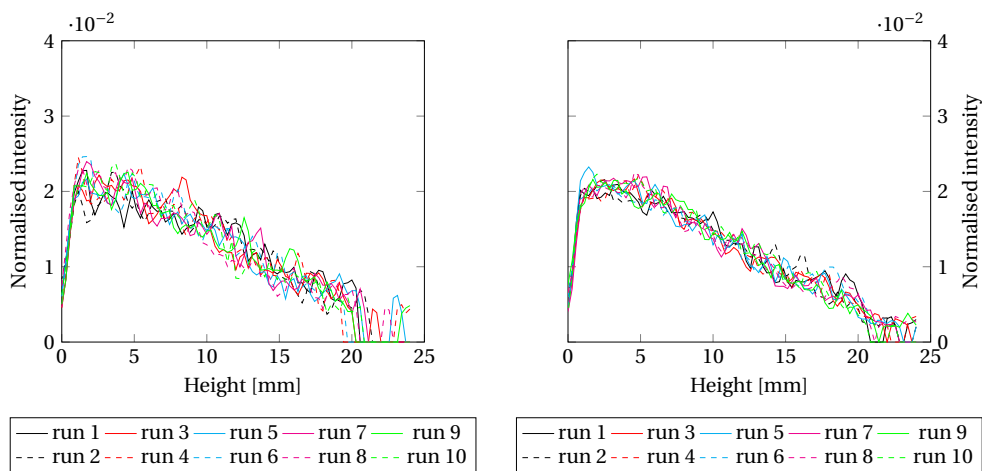

Figure B.12: Normalised intensity as a function of sample height obtained from low-field NMR after program modifications measured in 15 mm tube with $D5$ = 1 s with varying number of scans (ns). Left plot: ns = 8; right plot: ns = 16.